A MATHEMATICAL MODEL OF THE FLOW AND BED TOPOGRAPHY IN CURVED CHANNELS

Communications on Hydraulics

Report No. 85 - 1

Kim Wium Olesen

Laboratory of Fluid Mechanics

Department of Civil Engineering

Delft University of Technology

CONTENTS

SUMMARY

A two-dimensional horizontal mathematical model of the flow and bed topography in alluvial channel bends is presented. The applicability of the model is restricted to channels of which the width-depth ratio is large, the Froude number is small, bed load is dominant and grain sorting effects are negligible.

First order analyses of the mathematical model, using both steady and unsteady perturbations, are carried out, and an integration procedure based on a CSFT finite difference approximation of the mathematical model is outlined. Stability and accuracy of the numerical model are investigated.

Computational results are compared with data from two laboratory flumes and with data from a small natural river. The computed bed topographies and flow distributions agree rather well with the measured data, if the model is properly calibrated.

LIST OF SYMBOLS

a	coefficient in the model for the direction of the bed shear stress in a curved flow. See eq. (9).
b	exponent in the sediment transport model. See eq. (24).
d	characteristic grain size of the sediment.
f	or $f(\theta)$, "coefficient" in the sediment transport direction model. See eq. (8) and figure 1.
g	gravitational acceleration.
h	water depth.
n	curvelinear coordinate perpendicular to the river axis.
s	curvelinear coordinate parellel to the river axis.
t	time coordinate.
u	depth averaged flow velocity in s-direction.
v	depth averaged flow velocity in n-direction.
B	width of the channel.
C	Chézy roughness coefficient.
F_1	see eq. (36).
F_2	see eq. (36).
I	water surface slope.
L_s	wave length of bed deformation in s-direction (meander length).
P	pressure at the water surface (rigid lid).
Q	discharge
R	radius of curvature of s-coordinate line.
R_s	radius of curvature of streamline.
S_n	volumetric sediment flux including pores in n-direction.
S_s	volumetric sediment flux including pores in s-direction.
$\mathcal{f}$	or $\mathcal{f}(\theta)=f(\theta)/f(\theta_0)$. See eq. (17).
i	$=\sqrt{-1}$
j	$=n/\Delta n$. See eq. (31).
k	wave number in s-direction. See eq. (19).
k_B	wave number in n-direction. See eq. (19).

l $=2B/L_s$

m $=s/\Delta s$. See eq. (31).

o $=t/\Delta t$. See eq. (42).

p iteration number. See eq. (28).

Italic symbols not found in this list are normalized variables of the lower-case symbols, e.g. $h=h/h_0$.

α coefficient in sediment transport model (diffusion coefficient). See eq. (7).

γ numerical amplification factor. See eq. (41).

γ_p numerical amplification factor. See eq. (40).

γ_Δ numerical amplification factor. See eq. (39).

δ direction of the bed shear stress. See eq. (8).

δ^* angular difference between bed shear stress and depth averaged streamline in acurved flow. See eq. (9).

η $=k_B\Delta n$. See eq. (32).

θ Shields' parameter.

κ von Kármán's constant.

λ_s characteristic length scale of bed deformations. See eq. (17).

λ_w characteristic length scale of the main flow. See eq. (12).

λ_{sf} characteristic length scale of the secondary flow. See eq. (10).

ξ $=k\Delta s$. See eq. (32).

ρ density of the water.

ϕ amplification factor of linear analytical solution. See eq. (24).

ϕ_N amplification factor of linear numerical solution. See eq. (43).

ψ direction of the sediment transport. See eq. (8).

χ relaxation coefficient. See eq. (28).

Δ =1.65. Relative density of the sediment.

Δn Step size in n-direction of the computational grid.

Δs Step size in s-direction of the computational grid.

Δt Time step in computational model.

Subscripts

0	e.g. h_0 equilibrium value of variable in a straight river with the same width, roughness and discharge as the considered river.
'	e.g. h' perturbation variable.
^	e.g. $\hat{h}$ complex amplitude of a variable in the linear analytical solution
~	e.g. $\tilde{h}$ complex amplitude of a variable in the linear numerical solution

1. Introduction.

Bed level changes in straight as well as in curved alluvial rivers play an important part in several aspects of river engineering such as navigability, river regulation and bank protection. So far these problems were mostly studied by means of often expensive hydraulic scale models, even though the complex nature of the mutual interacting system of water and sediment unavoidably gives rise to serious scale effects (Struiksma et al., 1985). Therefore it is very attractive to attempt to develop a mathematical model and a numerical integration procedure which can replace or can be at least a valuable support for hydraulic scale models.

The development of a mathematical model for forecasting time dependent changes of flow and bed topography in curved alluvial rivers forms the major research object of the river bend group of the joint hydraulic research program TOW ("Toegepast Onderzoek Waterstaat"), in which Rijkswaterstaat (Governmental Water Control and Public Works Department), the Delft Hydraulics Laboratory and the Delft University of Technology participate. The present investigation is carried out at the Laboratory of Fluid Mechanics at the Delft University of Technology within the framework of the TOW river bend project. The investigation deals with an efficient integration procedure for a mathematical model for the time dependent flow and bed topography development in alluvial channels with vertical side walls, constant width and arbitrary alignment.

So far most attempts to predict the equilibrium bed topography in river bends have been based on local cross-sectional mean values of water depth, flow velocity and local radius of curvature (e.g. van Bendegom, (1947)), which, according to Struiksma et al.(1985), in most cases is not possible. The mathematical model developed by Engelund (1974) for the equilibrium flow and bed topography in rivers of which the curvature variation is given by a sine-function, was the first model including main flow inertia and continuity of the sediment transport (i.e. the sediment transport direction does not coincide with the river axis). The mainly analytical integration procedure suggested by Engelund is based on a linearized version of the mathematical model. However,one non-linear term is maintained and here numerical integration is applied. In spite of this non-linear term superposition is possible. So, by means of a Fourier series expansion, in principle the flow and bed level can be predicted in rivers with arbitrary alignment.

Other important intermediate steps towards the present model have been the extensive analysis of steady flow in curved rivers carried out by De Vriend (1981) and the development of a simplified mathematical model and integration procedure for two-dimensional horizontal flow by Kalkwijk & De Vriend (1980). This flow model accounts for longitudinal main flow convection, bottom friction, river curvature and, in case of mildly sloping banks, transverse convection of momentum by the secondary flow. Later, Olesen (1982 b) extended this model to account for the actual curvature of the flow in stead of the curvature of the river. Several scientists, among others van Bendegom (1947) and Engelund (1974 and 1981), have investigated the direction of the sediment transport on a sloping bed (for a review, see Odgaard, 1981), which is of essential influence on the bed topography in alluvial rivers. Finally, the linear analysis of the mathematical model for the flow and bed topography in straight rivers carried out by Olesen (1983), Struiksma (1983 a) and Struiksma et al.(1985) contribute to the understanding of the bed level development in (curved) rivers; and, in addition, it provides a powerfull tool for calibration of numerical models as the present one.

The applicability of the present model is restricted to rivers of which:

1. The width-depth ratio is large (shallow water approximation).

2. The Froude number is small (rigid lid approximation).

3. Bed load is dominant (the sediment transport rate can be determined

by means of local parameters only).

4. Grain sorting effects are negligible (no spatial variation of the sediment transport rate due to grain size variation).

Furthermore, in order to apply a uniform lateral step size in the numerical intergration procedure and to avoid curvature of the coordinate lines normal to the river axis, the width of the considered river must be approximately constant. However,this is not an essential assumption.

In the following the mathematical model will be summarized, the model will be linearized and the analytical solution of the linearized model for a double harmonic perturbation of the bed in a straight river will be derived. Next the integration procedure will be outlined and a von Neumann analysis, also for a straight river, will be carried out. Finally, the results of numerical computations are compared with data from flume experiments and with data from a small natural river.

2. Mathematical model.

The basic assumption underlying a mathematical model for the flow and bed topography in alluvial rivers is, that the flow can be considered quasi steady, i.e. the flow is assumed to adapt much faster to changes in bed level than the bed level changes itself. This permits a convenient distinction between steady flow computation and bed level computation.

The alignment of the rivers to be considered can be divided into curved sections, so it is obvious to apply a curvilinear coordinate system. This coordinate system has a s-axis coinciding with the channel axis and positive in the flow direction, a n-axis straight horizontal and perpendicular to the s-axis and a z-axis positive upwards. The local radius of curvature, R, of the coordinate system is by definition negative if the n-axis points towards the center of curvature. In this coordinate system the depth-averaged flow can be described by (cf. Kalkwijk & de Vriend, 1980)

$$\frac{\partial hu}{\partial s} + \frac{\partial hv}{\partial n} + \frac{hv}{R} = 0 \tag{1}$$

$$u\frac{\partial u}{\partial s} + v\frac{\partial u}{\partial n} + \frac{uv}{R} - \frac{1}{\rho}\frac{\partial P}{\partial s} + \frac{g}{C^2}\frac{u^2}{h} = 0 \tag{2}$$

$$-\frac{u^2}{R_s} + \frac{1}{\rho}\frac{\partial P}{\partial n} = 0 \tag{3}$$

in which

g acceleration due to gravity

h depth of flow

u,v depth averaged flow velocity in s- and n-direction, respectively

C Chezy roughness coefficient

P pressure at the water surface (rigid lid approximation)

R local radius of curvature of s-line. $R=R_a+n$, with R_a radius of curvature of river axis

R_s radius of curvature of streamline

ρ mass density of fluid.

According to de Vriend (1978) the streamline curvature can be approximated by

$$\frac{1}{R_s} = \frac{1}{R} - \frac{1}{u}\frac{\partial v}{\partial s} \tag{4}$$

Equation (1) is exact, whereas the momentum equations, eqs. (2) and (3), are based on some assumptions, namely: transverse convection of momentum by the secondary flow is negligible; the transverse main flow velocity is much smaller than the longitudinal one so terms with v^2 can be disregarded with respect to u^2; the pressure is hydrostatic, lateral friction is negligible and the transverse bed shear stress component can be disregarded.

The mathematical model of. the flow has a mixed hyperbolic /elliptic character (Olesen, 1982 b), which implies that conditions must be imposed at all boundaries. Impermeable side walls (v=0) provide two of the necessary conditions, a given inflow distribution the third one and several possibilities exist for the down-stream one. Mostly this condition is not known. The most simple solution is to prescribe $\partial v/\partial s=0$ at the outflow section. The computational results, concerning the flow and equilibrium bed level, are only influenced by the applied condition at the outflow section within a distance of approximatly one time the width of the channel.

Small Froude numbers permit the application of the rigid lid approximation. In that case the bed level can be replaced by the depth of flow in the mass balance equation for the sediment; viz.

$$\frac{\partial h}{\partial t} = \frac{\partial S_s}{\partial s} + \frac{\partial S_n}{\partial n} + \frac{S_n}{R} \tag{5}$$

in which

t time coordinate

S_s, S_n sediment transport rate in s- and n-direction, respectively.

By introducing the direction of the sediment transport, $\tan\psi$, the transverse transport component can be eliminated, viz.

$$\frac{\partial h}{\partial t} = \frac{\partial S_s}{\partial s} + \frac{\partial S_s \tan\psi}{\partial n} + \frac{S_s \tan\psi}{R} \tag{6}$$

A number of (semi-) empirical sediment transport models are known from the literature. In most of these models the sediment transport rate depends on the magnitude of the bed shear stress, but, for simplicity the transport rate is here considered to depend on the longitudinal flow velocity. In addition, it is convenient to apply a sediment transport formular that account for bed slope effects, i.e. the sediment transport rate is larger in case of down-hill slope than in case of a flat bed or up-hill slope. A sediment transport model with the slope effect included can, in the most simple way, be expressed like

$$S_s = S(u)\ (1 + \alpha\frac{\partial h}{\partial s}) \tag{7}$$

in which S(u) is the transport rate in case of uniform depth and α is a coefficient, probably depending on the sediment and flow properties. The major reason why the slope effect is included in the sediment transport model is that it provides some diffusion in eq. (6), which is very convenient for the numerical integration of the mathematical model. So far, the coefficient has not been experimental determined. Fortunately, the computational results are insensitive to the numerical value of α, if α is smaller than about 10, which is large enough to enable application of an atractive time step in the numerical integration procedure.

The boundary conditions for the bed level model are impermeable side walls (S_n=0) at n= B/2 and $\partial h/\partial t$=0 at the upstream boundary. At the outflow section the slope effect is omitted, viz. S_s=S(u).

Several models for the direction of the sediment transport are available (cf. Odgaard, 1981). The models are all based on the assumption that the gravitational force acting along an inclined bed causes a deviation of the transport direction from the direction of the bed shear stress. Most models have the form:

$$\tan\psi = \tan\delta + f(\theta) \frac{\partial h}{\partial n} \tag{8}$$

in which δ is the angle between the bed shear stress vector and the river axis and $f(\theta)$ is a weighing function of the Shields' parameter (θ). In figure 1 several suggested weighing functions are depicted. Equation (8) has not yet been sufficiently experimentally verified, i.e. independent measurements of all the quantities in the equation. So far $f(\theta)$ has mostly been obtained from curved flume experiments, in which it has been assumed that the sediment transport is parallel to the flume axis, (i.e. $\tan \psi=0$) in combination with a model for the direction of the bed shear stress in a curved flow. If the length of the arc of

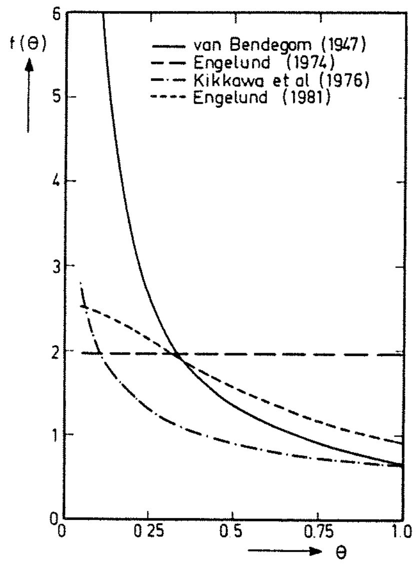

Figure 1. Models for the gravitational effect on the sediment.

the bend is much larger than the width then tan ψ=0 is a reasonable assumption, however, in most of the curved flume experiments, which have been used for verification of models for the gravitational effect, this was not the case. Another implication of this procedure for verification of f(θ) is that the reliability of f(θ) is limited by the reliability of the model for the direction of the bed shear stress.

The deviation angle between the bed shear stress vector and a depth averaged streamline in a curved flow with fully developed secondary flow is given by (Jansen, 1979)

$$\tan\delta^{*} = - a\frac{h}{R_s} \quad , \quad a = \frac{2}{\kappa^2}\left(1 - \frac{\sqrt{g}}{\kappa C}\right) \qquad (9)$$

in which κ is the Von Karman constant. This model does not apply close to the side walls. Some flow velocity data from smooth bed experiment show good resemblance with the theory reasonably close to the bottom. However, in case of a dune covered bed, it is hardly feasible to measure the direction of the flow close to the bottom sufficiently accurately, so in case of rough bed the model is not verified .

Rozowskii (1957), de Vriend (1981) and others suggested to describe the retarded adaption of the secondary flow to an abrupt change in its source by a damped exponential function with a relaxation length λ_{sf} = constant$\cdot C/\sqrt{g}\,h$. So, in case of a continous varying source, it is likely to assume that the adaption of the secondary flow and the bed shear stress due to the secondary flow can be described by

$$\lambda_{sf}\frac{\partial \tan\delta^{*}}{\partial s} + \tan\sigma^{*} = - a\frac{h}{R_s} \qquad (10)$$

The numerical value of the constant in the relaxation length for the secondary flow is encumbered with a great deal of uncertainty. The proper value of the constant for the bed shear stress is probably about 0.5-1, whereas the adaption of the secondary flow profile (intensity) demands a longer distance (cf. de Vriend, 1981 and Booij et al., 1982). In most cases the computed bed level is insensitive to the adaption length of the secondary flow, because the length scales of which main flow and bed topography changes takes place are much larger than the adaption length of the secondary flow (see Figure 2 and Struiksma et al., 1985).

Finally, also accounting for the deviation angle between the coordinate system and the streamlines, the direction of the sediment transport is given by

$$\tan\psi = \frac{v}{u} + \tan\delta^{*} + f(\Theta)\,\frac{\partial h}{\partial n} \qquad (11)$$

in which $\tan\delta^{*}$ must be obtained from eq. (10).

2.1. Normalization

In order to find out which parameters characterize the system of water and sediment and to get an insight into the relative magnitude of the various terms, the mathematical model described in the foregoing is normalized.

It is not quite evident which scale factors are adequate for the normalization of the whole model, however for the flow model it is natural to use the equilibrium depth, h_0 (in the following subscript 0 refers to the equilibrium value of the variable in a straight river with the same discharge, sediment transport and width as the river considered) the relaxation length of the main flow, $\lambda_w = C^2/(2g)\, h_0$, and the width, B, in z-, s- and n-direction, respectively. The flow velocity is scaled with u_0. Using these scale factors the mathematical model can, after combination of eqs. (3) and (4), be expressed in dimensionless form (italics) by

$$\frac{\partial hu}{\partial s} + \frac{\lambda_w}{B}\left(\frac{\partial hv}{\partial n} + \frac{hv}{R}\right) = 0 \tag{12}$$

$$u\frac{\partial u}{\partial s} + \frac{1}{2}\frac{u^2}{h} + \frac{\partial P}{\partial s} + \frac{\lambda_w}{B}\left(v\frac{\partial u}{\partial n} + \frac{uv}{R}\right) = 0 \tag{13}$$

$$u\frac{\partial v}{\partial s} + \frac{\lambda_w}{B}\left(\frac{\partial P}{\partial n} - \frac{u^2}{R}\right) = 0 \tag{14}$$

$$\frac{\partial h}{\partial t} = \frac{\partial S_s}{\partial s} + \frac{\lambda_w}{B}\left(\frac{\partial S_s \tan\psi}{\partial n} + \frac{S_s \tan\psi}{R}\right) = 0 \tag{15}$$

$$S_s = S\left(1 + \alpha\frac{h_o}{\lambda_w}\frac{\partial h}{\partial s}\right) \tag{16}$$

$$\tan\psi = \frac{v}{u} + \tan\delta^* + \frac{B}{\lambda_s} f(\theta)\frac{\partial h}{\partial n} \tag{17}$$

$$\frac{\lambda_{sf}}{\lambda_w}\frac{\partial \tan\delta^*}{\partial s} + \tan\delta^* = -\frac{a}{f(\theta)}\frac{B}{\lambda_s}\left(\frac{h}{R} - \frac{B}{\lambda_w}\frac{h}{u}\frac{\partial v}{\partial s}\right) \tag{18}$$

in which $\lambda_s = \left(\frac{B}{h}\right)^2 \frac{h}{f(\theta_0)}$ and, furthermore, the two following scale factors are introduced:

$$\mathrm{t} = t\ h_0\lambda_w/S_0$$

$$\mathrm{P} = P u_0^2 \rho$$

The normalized equations, (12) through (18), show that the equilibrium flow and bed topography depends on six quantities, viz.

$$\frac{B}{R},\quad \frac{\lambda_w}{B},\quad \frac{\lambda_w}{\lambda_s},\quad \frac{\alpha h_0}{\lambda_w},\quad \frac{\lambda_{sf}}{\lambda_w}\quad \text{and}\quad \frac{a}{f(\theta_0)}$$

and, of course, the (spatial) variation of the sediment transport rate, $S_s(u)$, and the variation of the gravitational term, $f(\theta)$.

The normalization has an interesting implication for scale models of rivers. Proper scale modelling requires that the six quantities are on scale one. It is mostly impossible to reproduce the alluvial roughness correctly in scale models. From λ_w/B on scale one it then follows that the model must be distorded; however, from $(\frac{\lambda_w}{B})/(\frac{\lambda_w}{\lambda_s})/(\frac{a}{f(\theta_0)} = \frac{B}{h\ a}$ it actually follows that the model must not be distorded (a is only weakly dependent on the roughness). Consequently, scale effects are unavoidable in this kind of scale models, provided the roughness is not on scale one (cf. Struiksma et al., 1985). In addition, $\alpha h_0/\lambda_w$ and λ_{sf}/λ_w depend strongly on the roughness coefficient, but the influence of these two quantities is modest.

2.2. Linear analyses.

In the following the linear analytical solution of the mathematical model, with B/R=0 (straight rivers), will be summarized. For a more profound description of the first part of the linear analysis (a stability analysis), see Olesen (1982 a). The linear solution can serve as a standard of reference for a von Neumann analysis of the numerical model and as standard of reference for computational results in case of small amplitude disturbances.

The linear solution is obtained by introducing perturbed variables, i.e. $u=1+u'$, $h=1+h'$ etc., into the normalized mathematical model neglecting quadratic and higher order terms. Furthermore the perturbations are assumed to be double harmonic, viz.

$$\begin{pmatrix} h' \\ u' \\ v' \end{pmatrix} = \begin{pmatrix} \hat{h} \\ \hat{u} \\ \hat{v} \end{pmatrix} \exp i\ (k\ s + k_B n - \phi t) \qquad (19)$$

in which $\hat{h}$, $\hat{u}$ and $\hat{v}$ are the dimensionless complex amplitudes of the perturbations, k and k_B are dimensionless wave numbers in s- and n-direction, respectively, $i=\sqrt{-1}$ and ϕ is a complex celerity in which the real part is the propagation velocity and the imaginary part is the exponential growth rate. The linear solution is unstable (growing) if the imaginary part of ϕ is positive.

The boundary conditions, impermeable side walls, puts constraints on k_B; viz.

$$k_B = \pi q \quad , \; q = 1,2,3 \; . \; . \; . \tag{20}$$

Inserting eq. (19) into the linearized version of eqs. (12), (13) and (14) leads to a set of equations from which the complex amplitudes of the flow velocities can be obtained. The amplitudes read

$$\hat{u} = \left[\frac{1}{2} - i \frac{k^3}{(k_B \lambda_w / B)^2} \right] / \left[1 + i(k + \frac{k^3}{(k_B \lambda_w / B)^2}) \right] \tag{21}$$

$$\hat{v} = - \frac{kB}{k_B \lambda_w} \left[\frac{3}{2} + i\, k \right] / \left[1 + i(k + \frac{k^3}{(k_B \lambda_w / B)^2} \right] \tag{22}$$

The amplitude of the streamline curvature is given by

$$\widehat{\frac{1}{R_s}} = \hat{i}\, k \frac{B}{\lambda_w} \hat{v} \tag{23}$$

Finally inserting eqs. (21), (22) and (23) into the linearized version of eqa. (15) through (18) yields an expression for the complex celerity; viz.

$$\begin{aligned} \phi = & - i(\frac{\lambda_w}{\lambda_s} k_B^2 + \frac{\alpha h}{\lambda_w} k^2) + k\Bigg[\frac{3-b}{2} + i(k + b \frac{k^3}{(k_B \lambda_w / B)^2}) \\ & + \frac{ah_0}{\lambda_w} \frac{i\, k}{1 + i\, k \lambda_{sf} / \lambda_w} (\frac{3}{2} + i\, k) \Bigg] / \left[1 + i(k \frac{k^3}{(k_B \lambda_w / B)^2}) \right] \end{aligned} \tag{24}$$

in which $b = \dfrac{u_0}{S_0} \dfrac{\partial S}{\partial u}$

Positive imaginary part of eq. (24), i.e. an unstable solution, is related to the occurrence of propagating alternate bars in straight channels. Maximum instability mostly occurs for wave length of two times the width in transverse direction (i.e. q=1 in eq. 20) and 3 to 5 times the width in longitudinal direction. The following factors promote the instability: increasing b and a h_0/λ_w and decreasing λ_w/λ_s, $\alpha h_0/\lambda_w$, λ_{sf}/λ_w and λ_w/B (cf. Olesen, 1982 a and 1983). Numerical computation for a case in the unstable region is of course excluded.

For some specific cases also the equilibrium solution can be obtained from the linear approach. The equilibrium solution is characterized by ϕ=0 in eq. (24). This leads to a sixth order polynomial in k. So, the solution is formed by a sum of six complex exponential functions for each possible value of k_B. For instance for the depth the solution reads

$$h' = \sum_{q=1}^{\infty} \hat{h}_q \exp i(\pi q n) \sum_{p=1}^{6} \hat{h}_{pq} \exp i(k_{pq} s) \tag{25}$$

recalling $k_B = q\pi$. From eq. (25) and v=0 at the walls the condition for existence of a linear solution of this sort can easily be derived; namely the boundary condition for the depth (and u , S_s) must be met by a Fourier serie consisting of only odd (i.e. q odd) sine functions and even cosine functions and vice versa for the boundary condition on v (and tan ψ). A sufficient condition herefore is that the boundary conditions fulfil

$$h'(n) = -h'(-n)$$

$$v'(n) = v'(-n)$$

and similar for the remaining variables.

Four of the six roots of the polynomial are purely imaginary characterizing four real exponential functions of which two are decaying and two growing. The two remaining roots mostly have the form: $k=\pm k_r + ik_i$ which characterizes two identical exponential damping or growing harmonic waves. In figure 2 the four imaginary roots and the real and imaginary part of the two complex roots are depicted as a function of

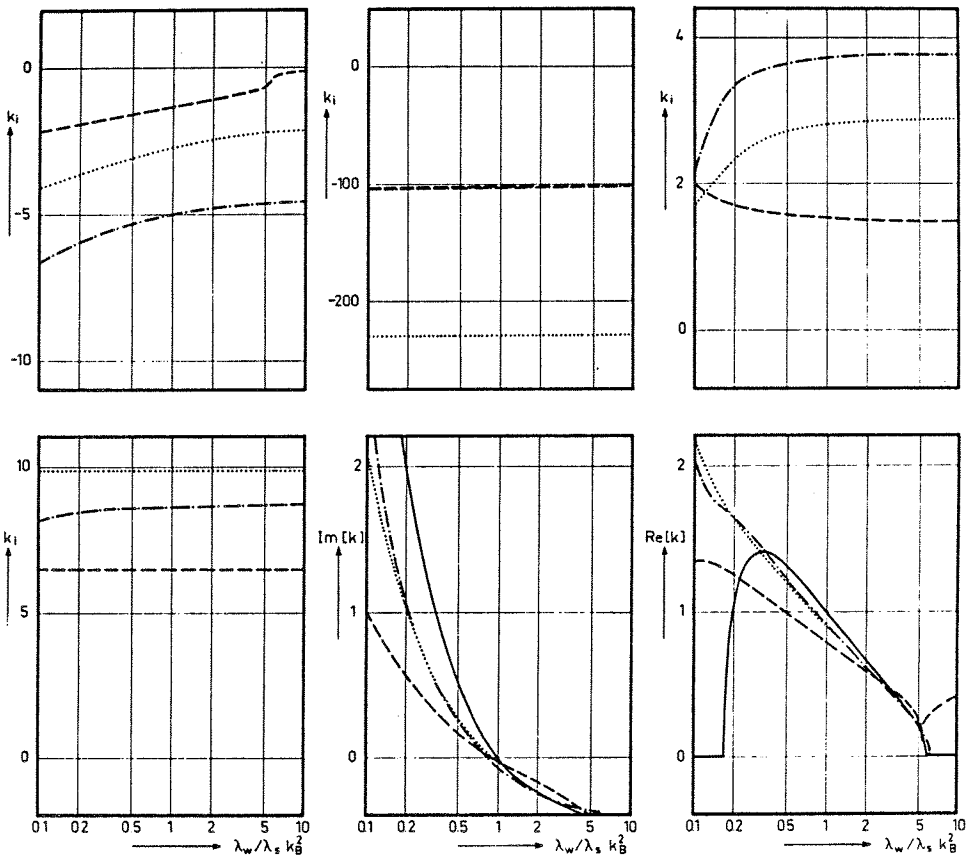

	$\alpha h_0/\lambda_w$	λ_{sf}/λ_w	$k_B\lambda_w/B$	$a h_0/\lambda_w$
– – – –	0.0491	0.157	2.56	0.126
–·–·–	0.0491	0.157	10.24	0.126
··········	0.0218	0.105	5.76	0.0593
———	Solution of Equation (27)			

Figure 2. Wave numbers of the linear solution.

$\lambda_w/\lambda_s k_B^2$.The absolute value of the four purely imaginary roots are generally much larger than the absolute values of the imaginary part of the two complex roots. This implies that the real exponential damped part of the solution only will be noticeable close to the upstream boundary, the exponential growing part close to the downstream boundary and that the harmonic part will be dominant in the central region of the considered area. Furthermore, generally the damping rate increases considerably for increasing q; so the first element of the Fourier series in eq. (25) will be dominant. Consequently, in a large part of the considered area, the linear solution can be approximated by

$$h' = \hat{h}_1 \sin(\pi n) \exp(-k_i s) \cos(k_r s + \text{phase}) \tag{26}$$

Equation (26) illustrates that the theory can be used for river planform classification and meander length estimation; viz. a river will tend to form meanders if a bed disturbance will grow (i.e.$k_i < 0$). The meander (arc) length is then given by $L_s = \lambda_w 2\pi k_r$ (cf. Olesen, 1983).

Struiksma (1983 a) (see also de Vriend & Struiksma 1983) drew up a simplified conceptual model in order to obtain a better insight into the processes which form the equilibrium topography in river(bends). He considered a straight river schematized into two parallel channels of constant width B/2 which are laterally connected so that water and sediment can be exchanged. In fact this model is more or less tantamount to eqs. (12) through (18) with 1/R=0, $\partial v/\partial s=0$ (no streamline curvature) and a=0 (no secondary flow). A linear analysis of this model leads to a quadratic polynomial reading

$$(k\,\lambda_w)^2 + (k\,\lambda_w)\; i\left[\frac{b-3}{2} - \frac{\lambda_w}{\lambda_s}\; k_B^2\right] - \frac{\lambda_w}{\lambda_s}\, k_B^2 = 0 \tag{27}$$

In figure 2 the roots of eq. (27) are also depicted. For a large range of $\lambda_w/\lambda_s k_B^2$ this model agrees qualitative rather well with the far more extensive analysis carried out above. Consequently, this simple model seems to include the main feature (i.e. retarded redistribution of flow and sediment transport) causing the wavy bed topography in rivers. Equation (27) demonstrates the large influence of the factor b; namely increasing b provides less damping, longer waves for small values of $\lambda_w/\lambda_s k_B^2$ and shorter waves for larger values of $\lambda_w/\lambda_s k_B^2$.

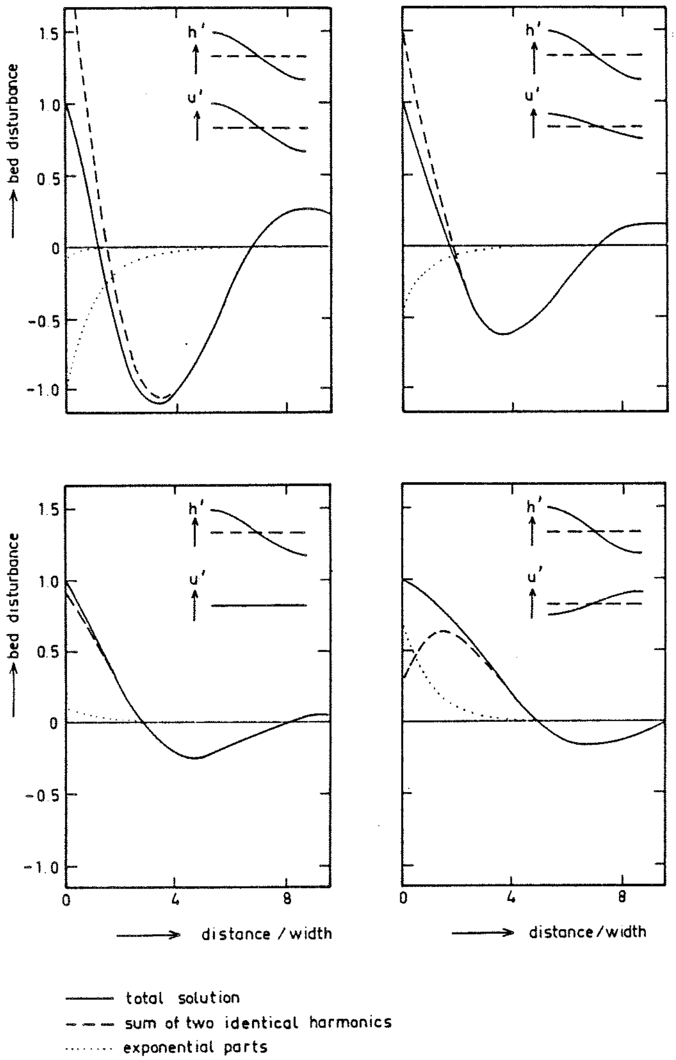

Figure 3. Decay of a bed level disturbance.

The linear analysis can be used to describe the development of a disturbance in any of the dependent variables. In figure 3 the decay along a side wall of a sine-formed (q=1 in eq. 20) disturbance at the upstream boundary of the depth is depicted for four different cases. The same disturbance of the depth has been used, whereas the perturbation of the longitudinal flow velocity differs in the four cases. The remaining dependent variables are undisturbed at the upstream boundary. The hydraulic and geometrical parameters originate from the DHL curved flume experiment described in chapter 4. In all four cases the solution consists of the same "sub-solutions". The figure can be considered as a schematized representation of the bed level immediately after the entrance of a bend (h'=0 in the axial symmetric solution in the bend) or after the exit of a bend (h'=0 in the equilibrium depth in the bend). So, with this simple linear solution it can be seen in which way the bed level in the first part of the bend (point bar height and pool depth) can be influenced. The figure suggests that it is important to have an accurate prediction of the flow field.

The wave lengths suggested by the analysis generally are much larger than the width of the river. It seems reasonable to assume that these long waves hardly are influenced by the magnitude of the two damping elements in the model, i.e. the relaxation length of the secondary flow (λ_{sf}) and the "longitudinal diffusion coefficient" (α), which also easily can be proved by means of the linear solution of the mathematical model. This is very convenient as large λ_{sf} and α provide the possibility to apply a large time step in the numerical integration procedure.

3. Integration procedure

In the present model, as in most morphological models, the bed level computation is devided into small time steps in which the bed is kept fixed and the flow considered steady. At each time step the steady flow field is computed from which the sediment transport rate is calculated and the bed configuration at the following time level is then obtained with an explicit finite difference approximation of the equation of continuity for the sediment. Stability requires application of a small time step in the integration procedure. This kind of model therefore involves a large number of bed level and steady flow computationsso a highly economical computation method is required.

In the following the integration procedure for the flow model and the bed level model will be shortly outlined and analyzed.

3.1. Integration procedure for the flow model.

Mostly, numerical solution of elliptic problems results in high costs because an, often large, matrix has to be inverted. In view of the mixed hyperbolic/elliptic mathematical character of the flow model high computational costs could also be expected for the present model, but a very economical integration procedure, which does not involve inversion of any matrix, is applied.

This efficient integration procedure is in principle based on the method suggested by Kalkwijk & de Vriend (1980). In this model, however, the streamline curvature is approximated by the local curvature of the coordinate lines resulting in a purely hyperbolic mathematical character. This permits a straight forward marching integration procedure with an implicit finite difference scheme, but Kalkwijk & de Vriend suggested an iterative procedure with an explicit scheme, which appears to be far more economical. The basic principle in this procedure is that terms with the tranverse main velocity is considered to be known: with a first guess for the transverse flow velocity (e.g. v=0) the longitudinal flow velocity can be obtained from eqs. (2) and (3) with a constant discharge as boundary condition. Next, the continuity equation (1) can be applied to obtain an improved estimate for the transverse flow velocity; and as many iterations can be made as accuracy requires. This integration procedure is unconditionally stable.

Later Olesen (1982 b) extended this model with an improved approximation for the streamline curvature, i.e. eq. (4). In the integration procedure the same basic principle is applied, but now also the streamline curvature is improved in each iteration step. In this case stability problems require a underrelaxation, viz. only a certain part of the new calculated streamline curvature is taken into account in the following iteration step. For instance, the streamline curvature applied in iteration number p is given by

$$\left(\frac{1}{R_s}\right)_p = \chi\left(\frac{1}{R} - \frac{1}{u}\frac{\partial v}{\partial s}\right)_{p-1} + (1-\chi)\left(\frac{1}{R_s}\right)_{p-1} \qquad (28)$$

in which χ is a relaxation coefficient. The relaxation coefficient which ensures stability reads

$$\chi < 8\left(\frac{\Delta s}{B}\right)^2 \qquad (29)$$

Experience with the model learns that the most efficient value is about

$$\chi = \max\left[4\left(\frac{\Delta s}{B}\right)^2 ; \frac{1}{2}\right] \qquad (30)$$

In view of eqs. (29) and (30), the integration procedure does not seem practicable for variations taking place on length scales shorter than the width of the river, as the relaxation coefficient then will become inconvenient small and hence the computational costs will be high. Fortunately, in the present case of alluvial rivers bed level and curvature variation normaly take place on length scales larger than the width.

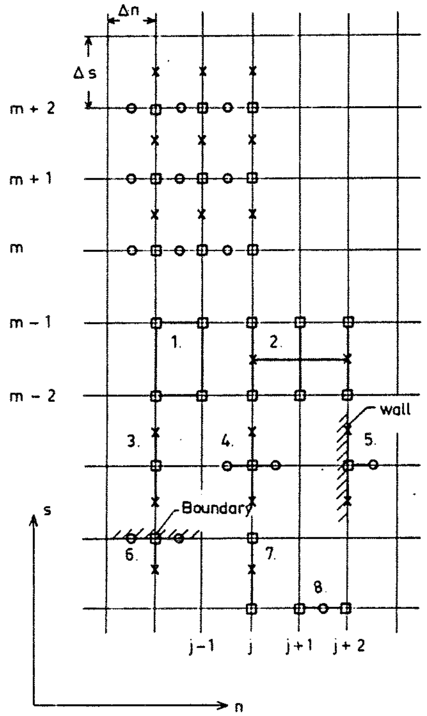

□ h, u, and $\frac{1}{R_s}$
x v, S_x and tan δ
o tan ψ and S_y

1. Eqs (2) and (3) combined
2. Eq. (1)
3. Eq. (4)
4. Eq. (6)
5. Eq. (6) - side wall
6. Eq. (6) - downstream boundary
7. Eq. (7)
8. Eq. (8)

Figure 4. Computational grid and finite difference approximations.

A staggered computational grid is applied (cf. figure 4). This grid allows a discretization of the equations with central differences and relative short space steps. Eqs. (2) and (3) are discretized into simple central differences from which the pressure is eliminated. This results in a box-scheme (the pressure can also be eliminated directly from eqs. (2) and (3), but the elaboration is somewhat more comprehensive because the succession of cross-differentiation is essential in the applied coordinate system). Eq. (1) is discretized in a kind of Stone and Brian scheme and eq. (4) is a simple central difference. The various finite difference schemes are depicted in the computational grid in figure 4. The discretization is outlined in details in Olesen (1982 b).

Generally the accuracy of a non-linear numerical model as the present one is not predictable; however, an analysis of the linearized model gives a good estimate of the order of magnitude of the accuracy of the non-linear model. Such a linear numerical analysis (von Neumann analysis) is quite similar to the linear analysis outlined in the previous chapter. The difference is that a discrete wave, defined in the grid points, is considered in stead of a continuous one. The von Neumann analysis is also carried out for a straight channel which formally implies that the analysis informs about the accuracy due to depth variations but not due to curvature variation.

The steady perturbation considered in the numerical analysis of the flow model reads

$$h = \tilde{h} \ \exp i \ (m \, \Delta \, s \, k - j \, \Delta n \, k_B) \tag{31}$$

in which $\tilde{h}$ is the amplitude of the depth perturbation, Δs and Δn are step lenghts in the computational grid and $m = s/\Delta s$ and $j = n/\Delta n$. The perturbations of the remaining variables have a similar form. The variables are normalized as outlined in chapter 2.

Discretization of eqs. (13) and (14) in the box scheme (cf figure 4) in combination with eq. (31) yields an expression for the complex amplitude of the longitudinal flow velocity, viz.

$$\tilde{u}_p = -\tfrac{1}{2}\left[\left(\frac{\tilde{f}}{R_s}\right)_p \Delta n \frac{\tan \xi/2}{\tan \eta/2} - \tfrac{1}{2}\,\Delta s\right]\left[i \tan \xi/2 + \tfrac{1}{2}\,\Delta s\right]^{-1} \tilde{h} \tag{32}$$

in which $\xi = k\Delta s$ and $\eta = k_B \Delta n$.

Equation (12) and the expression for the streamline curvature eqs. (28) discretized in the Stone and Brian scheme and in the simple central difference, respectively, gives expressions for the complex amplitudes of the remaining dependent variables, namely

$$\tilde{v}_p = -\tfrac{2}{3}\,\frac{B}{\lambda_w}\,(\tilde{u}_p + \tilde{h})\,\frac{\Delta n}{\Delta s}\,\sin\frac{\xi}{2}\,\frac{\cos\eta + 2}{\sin\eta} \tag{33}$$

$$(\frac{\tilde{1}}{R_s})_{p+1} = \chi \frac{B}{\lambda_w} \frac{2i}{\Delta s} \sin \frac{\xi}{2} \tilde{v}_p + (1 - \chi) (\frac{\tilde{1}}{R_s})_p \tag{34}$$

Combining the eqs. (32) through (34) gives a difference equation for the complex amplitude of the streamline curvature. The corresponding differential equation reads

$$\frac{\partial}{\partial p} (\frac{\tilde{1}}{R_s})_p = - \chi \left[F_1 (\frac{\tilde{1}}{R_s})_p - F_2 \right] \tag{35}$$

with

$$F_1 = 1 + \frac{2i}{3} (\frac{B}{\lambda_w} \frac{\Delta n}{\Delta s})^2 \left[\tan \frac{\xi}{2} \sin^2 \frac{\xi}{2} \frac{\cos\eta + 2}{\sin\eta} \right] \left[i \tan \frac{\xi}{2} + \frac{\Delta s}{2} \right]^{-1} \tag{36}$$

$$F_2 = \frac{2i}{3} (\frac{B}{\lambda_w})^2 \frac{\Delta n}{\Delta s^2} \left[(\frac{3\Delta s}{2} + 2 i \tan \frac{\xi}{2}) \sin^2 \frac{\xi}{2} \frac{\cos\eta + 2}{\sin\eta} \right] \left[i \tan \frac{\xi}{2} + \frac{\Delta s}{2} \right]^{-1} \tag{37}$$

The solution of the differential equation, eq. (34), with $1/R_s = 0$ as initial condition reads

$$(\frac{\tilde{1}}{R_s})_p = \frac{F_2}{F_1} \left[1 - \exp(- \chi F_1 p) \right] \tilde{h} \tag{38}$$

Similar expressions can be obtained for $\tilde{u}$ and $\tilde{v}$. A necessary condition for stability of the integration procedure is $\mathrm{Re}[F_1] > 0$, which, according to eq. (36), allways applies.

According to eq. (38) numerical inaccuracy can have two causes; namely, the exponential function still has a finite value, i.e. an insufficient number of iteration is carried out, and the end value of the iteration process, F_2/F_1, differs from the analytical solution (eq. (23)) due to a too rough discretization. As a measure for the accuracy the following quantities are introduced:

$$\gamma_\Delta = \frac{F_2}{F_1} \tilde{h} \, / \, (\frac{\hat{1}}{R_s}) \tag{39}$$

$$\gamma_p = 1 - \exp\,(\chi F_1 p) \tag{40}$$

$$\gamma = \gamma_\Delta\, \gamma_p \tag{41}$$

i.e. γ_Δ gives the numerical error due to the discretization and γ_p the error due to the number of iterations.

The magnitude of the amplitude error appears to play a larger role than the magnitude of the phase error for the over-all accuracy of the model. Consequently, design of a computational grid and choice of the number of iterations must be based on considerations about the magnitude of $|\gamma_\Delta|$ and $|\gamma_p|$, respectively.

In figure 5 the variations of γ_Δ with the discretization in transverse and longitudinal direction are depicted. The wave length in transverse direction is assumed two times the width, i.e. q=1 in eq.(20), which is the relevant wave length in most meandering alluvial rivers. The parameter l gives the ratio between the wave length in traverse and longitudinal direction, i.e. l=2B/L_s. Furthermore, B/λ_w=0.6, which is a

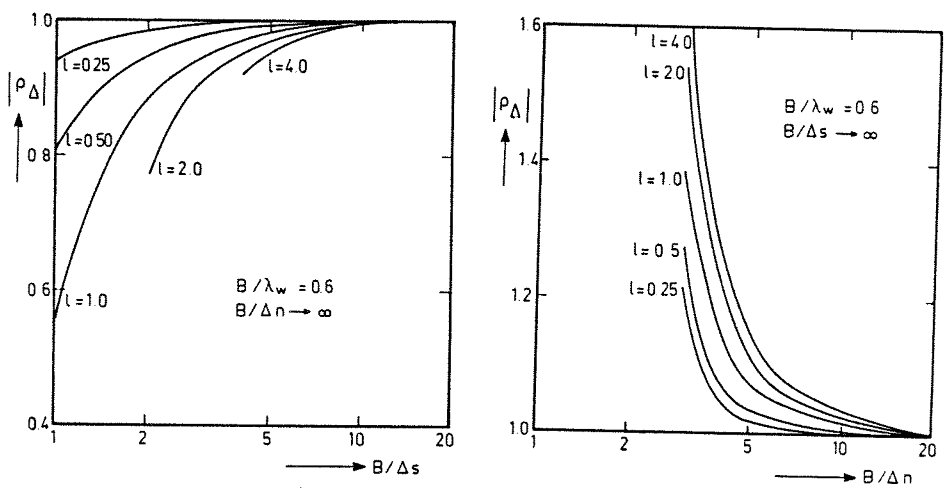

Figure 5. Discretization error.

representative value (the result of the analysis depends slightly on the value of B/λ_w). The figure shows that a finite discretization in transverse direction tends to overestimate the amplitude of the perturbation, whereas a finite discretization in longitudinal direction tends to underestimate it. Consequently, the discretization error in longitudinal and transverse direction will to some extent compensate each other.

In figure 6 a diagram is worked out, which indicates the necessary number of iterations to obtain an accuracy of 2 % as a function of the discretization in longitudinal direction; i.e. for given $B/\Delta s$ the quantity γ_Δ is calculated and the number of iterations for which $|1-\gamma_\Delta \gamma_p|=0.02$ is determined. The figure shows that neither short waves nor long waves cause much problems, whereas waves in longitudinal direction of the same length as the transverse waves demand a large number of iterations. Furthermore, if both short and long waves must be computed accurately then the number of necessary iterations is large. In

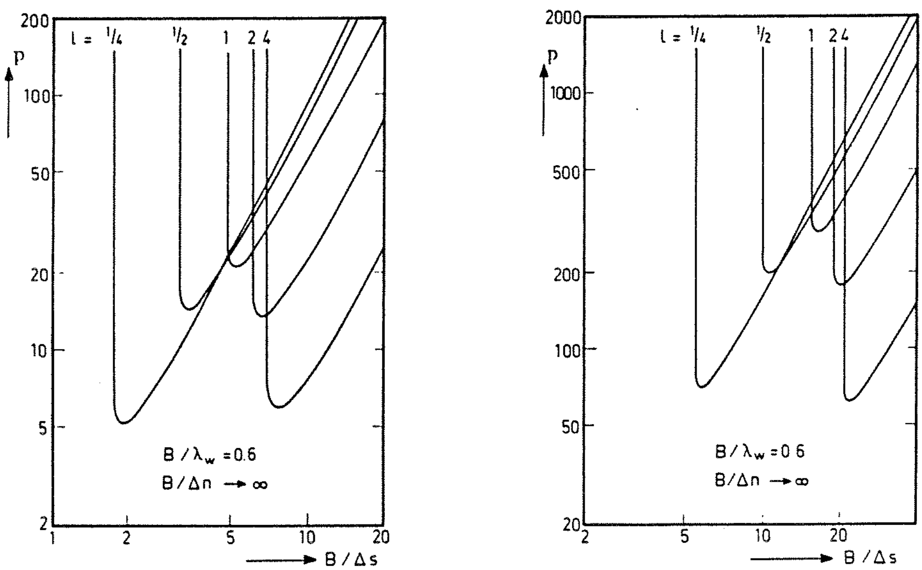

Figure 6. Discretization and iteration error (left: 2%, right: 0.2%).

figure 6 also a similar diagram for an accuracy of 0,2 % is depicted. Comparing this diagram with the one for an accuracy of 2% it appears that for $\tilde{l}=1$ an increase of the accuracy with a factor 10 demands a computational effort which is about 45 times larger. (p=21 and $B/\Delta s=5$ for an accuracy of 2 % and p=280 and $B/\Delta s=17$ for 0.2 %). It should be emphasized that figure 6 gives a conservative estimate of the accuracy of the model as the compensation due to the discretization in transverse direction is neglected.

Generally, the large scale bed forms in alluvial rivers have wave lengths which are considerably longer than the width of the river (cf. figure 2). Consequently, the numerical flow model is rather efficient for this case and therefore well suited for incorporation in a model for the bed topography in alluvial rivers. In case of rivers with short wave (non-alluvial) disturbances the flow velocity rather than the streamline curvature is mostly of interest and therefore, as the flow velocity is rather insensitive to the streamline curvature (cf Olesen, 1982 b), only few iterations are required. So the numerical model may also be sufficiently efficient for this kind of problems.

3.2. Integration procedure for the bed level model

The numerical solution of the bed level model is straightforward, i.e. a central space-forward time (CSFT)-difference approximation is applied. In appendix A the discretization is outlined in detail and the various finite difference schemes are depicted in the computational grid in figure 4.

A von Neumann analysis of the bed level model follows the same procedure as mentioned before, except in this case also time dependence of the variables must be considered. For instance the perturbation of the depth of flow reads

$$h^{a}_{m,j} = \tilde{h} \exp \; i(k\, m\, \Delta s + k_B j\, \Delta n - \phi_N\, O\Delta t) \tag{42}$$

in which ϕ_N is the numerical amplification factor and $t=o\Delta t$. Discretizing the linearized bed level model as described in appendix A, yields an expression for the numerical amplification factor, reading

$$\frac{\exp(-\,i\,\phi_N\,\Delta t)-1}{\Delta t} = \frac{b}{\lambda_w \Delta s}\; i \sin \; \frac{\tilde{u}}{\tilde{h}}$$
$$+ \frac{i}{B\Delta n} \cos\frac{\xi}{2}\,\left(1 + \frac{a}{\lambda_{sf} - i\,\lambda_w \Delta s/2\,\cot\frac{\xi}{2}}\right) \sin\; \frac{\tilde{v}}{\tilde{h}} \tag{43}$$
$$+ \frac{2\alpha}{(\lambda_w \Delta s)^2}\,(\cos\xi - 1) + \frac{2f(\theta)}{(B\Delta n)^2}\,(\cos\eta - 1)$$

in which $\tilde{u}$ and $\tilde{v}$ can be obtained from the analysis of the flow model, i.e. eqs. (32) and (33) in combination with eq. (38). In the following it will be assumed that so many iterations in the flow model are carried out that the significant part of the error in the flow solution is due to the discretization. In practice, however, only one iteration, except in the first flow computation, is carried out, i.e. the streamline curvature belonging to the bed level and flow at t-Δt is used to calculate the flow at t.

Stability of the integration procedure requires

$$\text{Im}\,\left[\phi_N\right] < 0 \tag{44}$$

Equation (43) is not very transparant and it is not easy to derive a stability criterion from this expression. It appears that three kinds of wave patterns can cause stability problems, viz: short waves in transverse direction; short waves in longitudinal direction and waves, in longitudinal direction, of the length 2 to 5 times the width. Combinations of these waves can also occur. The short wave instability is probably related to a sort of CFL-criterion, i.e. $\Delta s/\Delta t < C_s(..)$ and $\Delta n/\Delta t < C_n(..)$ where C_s and C_n are celereties. This kind of instability

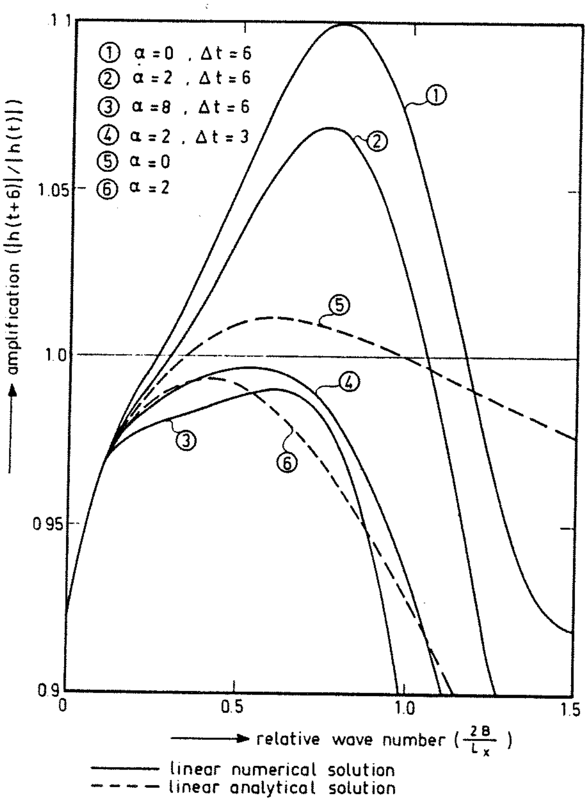

Figure 7. Comparison of unsteady linear numerical and linear analytical solution.

can be avoided by increasing the space step or decreasing the time step. In some cases short waves in longitudinal direction can also be damped by increasing the longitudinal diffusion coefficient α . The last kind of instability is not entirely a numerical problem; it is partly caused by instability of the mathematical model (alternate bars, cf. eq. (24), Olesen, 1982 a and 1983). This kind of instability can be avoided to some extent by increasing the diffusion coefficient α and reducing the time step. This is illustrated in figure 7 where the linear mathematical and linear numerical solution for a specific case (discretization and hydraulic parameters as in the computation for the DHL curved flume, see chapter 4) is compared for different α and Δt. The figure also shows that the agreement, concerning decay/growth of a bed disturbance, is relative poor especially for short waves. Accurate numerical treatment of these short waves demands a finer computational grid. A quite similar result applies for the propagation velocity of bed disturbances.

For a chosen grid spacing the stability analysis yields a maximum time step, however, if non-linear effects or spatial variation of the zero-order solution are significant (as in a river bend), then a time step of about the half of the step-size suggested by the stability analysis proved to be necessary in order to ensure stability.

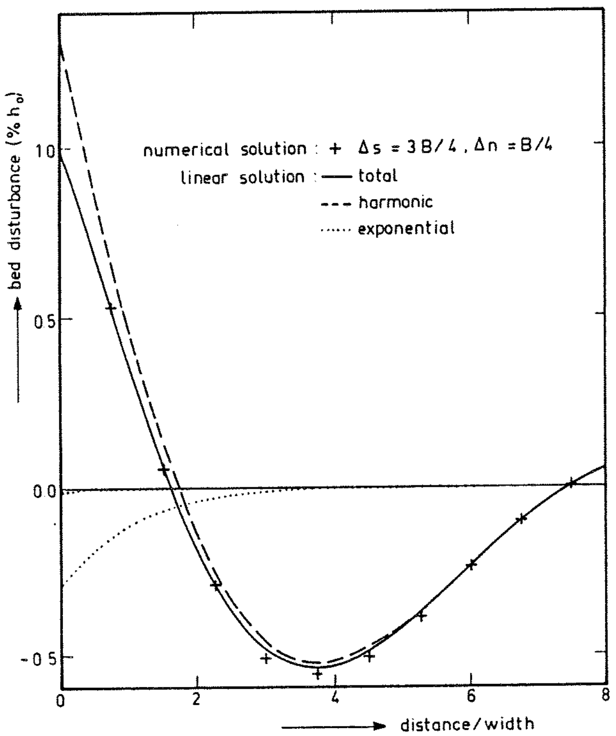

Figure 8. Comparison of numerical and analytical steady solution (coarse grid).

The accuracy of the integration procedure for time dependent processes can, as illustrated in figure 7, be obtained by comparing the linear mathematical solution with the result of the von Neumann analysis. Often only the equilibrium solution is of major interest. In this case the von Neumann analysis is not applicable as predictor for the accuracy, but the steady linear analytical solution can be compared with numerical computation of a small amplitude perturbation of the boundary condition in a straight river. In figures 8 and 9 the results of such comparisons are depicted.

The disturbance of the depth at the upstream boundary is sineous-formed with a wave length of two times the width (q=1 in eq. 20) and an amplitude of 1 % of the mean depth. The longitudinal flow velocity at

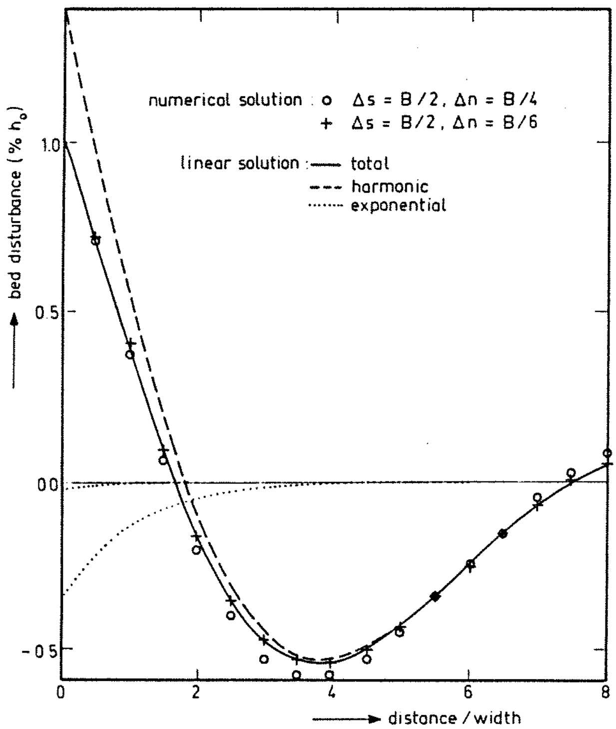

Figure 9. Comparison of numerical and analytical steady solution (fine grid).

the upstream boundary is distributed according to Chezy's law, i.e. sineous-formed with an amplitude of about 0.5 % of the mean flow velocity. The remaining variables are uniform at the boundaries. Due to the staggered computational grid the upstream boundary condition for the transverse main flow velocity and the magnitude of the secondary flow are imposed at $s=-\Delta s/2$. This implies that the numerical and analytical solution will differ slightly for different longitudinal space steps. The downstream boundary conditions for the analytical model are $\partial h/\partial s=0$ and $1/R_s=0$ for $s=\infty$. In the numerical computations this is simulated by taking $\partial^2 h/\partial s^2=0$ and $\partial(1/R_s)/\partial s=0$ at some distance downstream of the considered area.

In figure 8 the linear analytical and the computational results in the form of the development of the perturbation of the depth of flow along one of the banks are depicted. The analytical solution is clearly dominated by the harmonic part; but the purely exponential parts of the solution is not insignificant as it provides an initial amplitude of the harmonic part (phase) which is larger than the amplitude of the total disturbance (cf. figure 3). The numerical computation with $\Delta s=3/4B$ and $\Delta n=B/4$ provides a rather good accuracy.

In figure 9 it is attempted to improve the accuracy by reducing the longitudinal space to B/2 (note that the analytical solution is slightly altered), using the same transverse space step, but this leads to a more inaccurate numerical result. If, in addition, also the transverse space step is decreased then the accuracy is again improving. This illustrates that the accuracy is not only influenced by the individual magnitude of the space steps but also by the ratio between the two space steps. This phenomena corresponds well with the result of the von Neumann analysis of the flow model (cf. figure 5).

Quite a lot of computational effort can be saved by taking this phenomena into account. For instance, the costs of the numerical computation in figure 8 is only about 40 % of the costs of the computation with the fine grid in figure 9.

Figure 8 indicates that a surprisingly low number of computational grid points is necessary in order to obtain a good accuracy. Usually, a space step of B/4 to B/6 in transverse direction and B/2 to B in longitudinal direction provides excellent accuracy of the equilibrium solution. The final choice of a grid spacing, time step and diffusion coefficient must depend on a balance between computational expenses and required accuracy.

4. Computational results.

In the following results of numerical computations will be compared with results of bed topography measurements in two different flume experiments with well-defined steady flow conditions and with data from a small natural river. The comparison will only concern the equilibrium bed topography. In table 1 the measured hydraulic and geometrical properties for the three cases are summarized. The computational "details" such as time steps, space steps and model parameters, which have not been measured, are summarized in Appendix B.

The flume experiments have been selected for their distinct mutual differences in planform. The first case concerns a flume experiment carried out in a sineous-formed flume. This case provides the possibility to compare the computational results with both the measured data and with the solution of a simplified model suggested by Engelund (1974). The second case concerns an experiment carried out in a flume consisting of a short straight in-flow section followed by a long mildly curved bend and a short straight out-flow section. The final

			Hooke's flume exp.	DHL curved flume	the river Dommel
Discharge	Q	(m^3/s)	0.035	0.047	1.65
Width	B	(m)	1.0	1.5	5.0
Water depth	h	(m)	0.095	0.08	0.60
Flow velocity	u	(m/s)	0.37	0.39	0.55
Water surface slope	I	(‰)	2.21	2.36	0.56
Chézy coefficient	C	($m^{\frac{1}{2}}/s$)	25.4	28.4	30.0
Medium grain size	d_{50}	(mm)	0.30	0.45	0.47
Gradation parameter	σ_g	(-)	1.23	1.19	?
Bend radius (min)	R	(m)	1.46	12.0	11.0
Froude number	F	(-)	0.38	0.44	0.43
Shields' parameter	θ	(-)	0.42	0.26	0.43

Table 1. Hydraulic and geometrical properties.

case, a natural river, will illustrate some of the additional problems occurring when the model is applied to prototype cases.

4.1. Meandering flume

The first case concerns an experiment carried out at the University of Uppsala, Sweden, by Hooke (1974) in a meandering flume (cf. figure 10). The planform of the flume, the depth width ratio and Shields' parameter in the experiments were designed according to a large number of observations of natural rivers. A rather uniform sand was applied in order to avoid grain sorting effects (cf. table 1).

The bed topography was obtained from a single sounding after smoothing out the bed forms by hand. This may have introduced some uncertainty into the measured data. Hooke presented the bed topography in the form of a contour map; in the present report, however, it will be presented as longitudinal bed profiles, which have been obtained from the contour maps. This may have introduced some additional uncertainty into the data. In the experiment also the angular difference between flow at surface and flow near the bottom, the sediment transport distribution and the bed shear stress (magnitude) distribution were measured. According to Engelund (1974) the sediment transport and bed shear stress distribution suggest that the sediment transport is proportional to u^4. This sediment transport model will be maintained in the following.

No abrupt change of curvature takes place and therefore no steady bed deformations with short wave length occur. Consequently, a coarse computational grid in combination with a large diffusion coefficient (α), which permits large time steps, would provide sufficient accuracy. Nevertheless, a rather fine computational grid is applied in the numerical computations (cf. Appendix B), as it is convenient to have a large density of data for the preparation of figures.

4.1.1. Comparison with Engelund´s model

Allready in 1974 Engelund presented results of an integrated mathematical model for the equilibrium flow and bed topography in rivers of which the curvature variation is harmonic. The main difference between Engelund´s mathematical model and the present one is that the streamline curvature is approximated by the local channel curvature whereas equation (4) is used in this model. The remaining difference is that secondary flow inertia, slope dependence of the longitudinal transport rate and some small (second order) inertia terms in the flow model are neglected in the Engelund-model. The integration procedure suggested by Engelund is partly linear, but he maintains the probably most important non-linear variation. As an auxiliary condition for the integration procedure Engelund suggested to apply a constant cross-sectional mean depth along the channel. The appropriate condition at that point of the integration is that the sediment transport integrated over the width is constant along the river.

In figure 10 results of the measurements are compared with results of the numerical model and the Engelund model. The trend in the two computations is the same, i.e. the point bar and pool are situated downstream of the apex of the flume, however a distinct lag is observed. The position of the pool and point bar is rather good predicted by the Engelund model, whereas the point bar height and pool depth are slightly underestimated. The result of the Engelund model exhibits the best agreement with the measured data, however, this must to some extent be attributed to the choice of model parameters, that have been calibrated on the measured data with the Engelund model.

In order to attempt to isolate the cause of the distinct difference between the two computational results in figure 10 a numerical computation with the streamline curvature approximated by the local channel curvature and without secondary flow inertia was carried out.

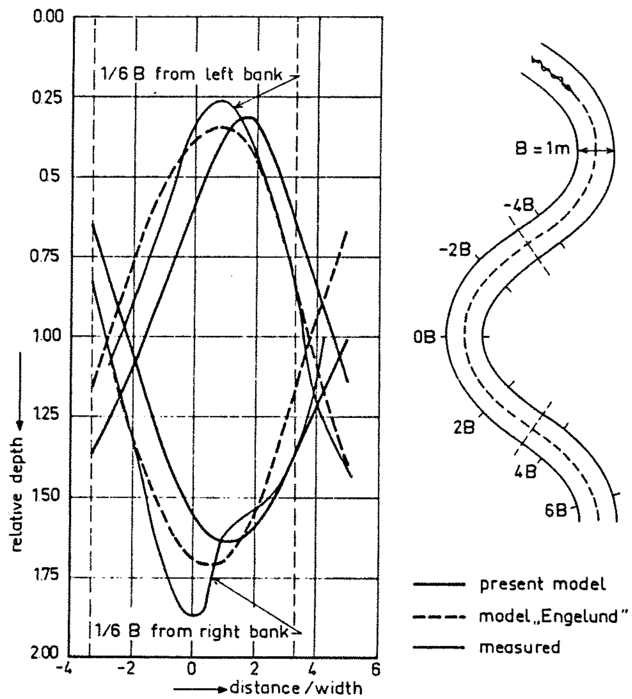

Figure 10. Comparison of computational result with model "Engelund" and with the measured data.

In figure 11 the result of this computation is compared with the Engelund model showing that the point bars are in phase and only a small distance lag between the pools. The Engelund model results in the most pronounced bed deformation. The difference between the two models in figure 11 is much smaller than the difference in figure 10. Computations with different relaxation length of the secondary flow showed that the bed topography is nearly independent of the relaxation length of the secondary flow so the streamline curvature approximation in the Engelund model is the major reason for the quantitative difference between the two models. The streamline curvature approximation used in the present model, i.e. eq. (4), can easily be incorporated in the Engelund model.

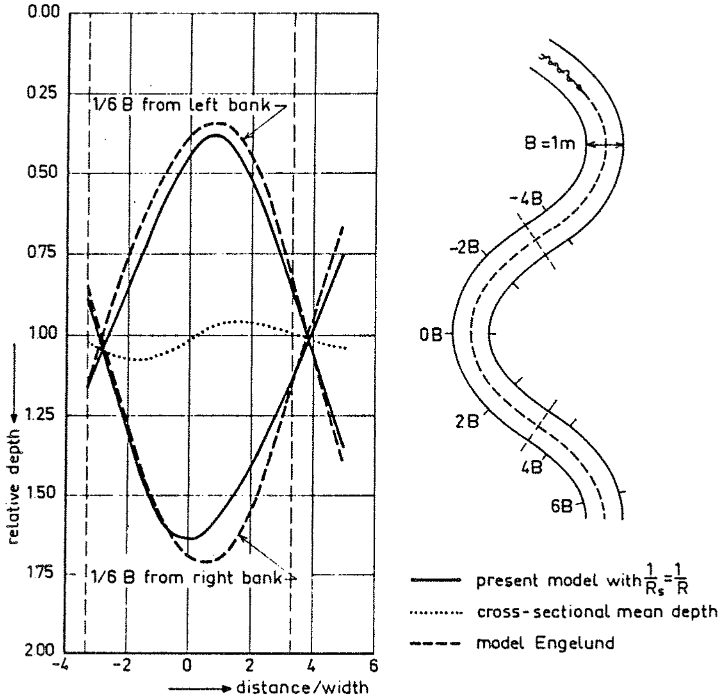

Figure 11. Comparison of the present model with the streamline curvature approximated by the channel curvature with model "Engelund".

The difference between the results of the two models in figure 11 must be attributed to two causes, viz. - the application of the auxiliary condition in the Engelund model and to non-linear effects. In order to estimate the influence of the auxiliary condition the cross-sectional mean depth, as computed by the non-linear model, is also depicted in figure 11. Applying this variation in stead of a constant mean depth as auxiliary condition in the Engelund model would lead to a slight shift upstream of the point bar and the pool, resulting in a better over-all agreement between the two models. Surprisingly the influence of the non-linearity is seen to moderate the bed deformations.

Consequently, the Engelund model, extended with equation (4) for the streamline curvature, will in many cases provide a sufficient accurate solution of the mathematical model. Application of this model is very attractive because the computational costs are much smaller than the costs with the non-linear time dependent numerical model. As the Engelund model permits superposition of different harmonics any river planform with constant width can be considered with this model; however, in case of a complex planform or an abrupt change of curvature of the considered river, extremely many harmonics must be considered and in this case the numerical model will probably appear to be most efficient. In addition, the Engelund model has the important disadvantage that it cannot treat unsteady conditions.

4.1.2. Calibration of the model

From the normalized equations, eqs. (12) through (16), it followed that the solution of the mathematical model only depends on six quantities and on the spatial variation of the sediment transport and of the term accounting for the bed slope effect on the sediment transport direction (cf. p. 10). In the present case only a few of these quantities are available for calibration purpose as the remaining quantities have been either directly or indirectly measured. Actually, only λ_s (i.e. $f(\theta_0)$ in eq. 8) and the spatial variation of $f(\theta)$ (figure 1) can be used for calibration.

The influence on the bed topography of the spatial variation of the term accounting for the bed slope effect on the sediment transport direction can easily be investigated. Assuming that $f(\theta) = \text{constant} \cdot \theta^{-p}$ (i.e. p=0 Engelund, 1974, p=1/2 Kikkawa et al., 1976 and p=1 Van Bendegom, 1947) then the transverse depth variation in a fully developed bend (i.e. v=0 and $\tan \psi = 0$ in eq. (11), which does not occur in the present case), can be approximated with a Taylor serie expansion into

$$h/h_{axis} = 1 + \frac{a}{f(\theta_0)} \left(\frac{n}{R}\right) + \frac{p+1}{2} \frac{a}{f(\theta_0)} \left(\frac{a}{f(\theta)} - 1\right)\left(\frac{n}{R}\right)^2 + \cdots \quad (45)$$

Consequently, the influence of the spatial variation of $f(\theta)$ is only of significant importance in case of sharply curved bends. Equation (45) also illustrates the influence of $a/f(\theta_0)$ on the fully developed bed topography, viz. the transverse bed slope is approximately proportional with $a/f(\theta_0)$. The linear analysis (cf. figure 2) shows the influence of $f(\theta_0)$ in case of developing bed deformations, namely the wave length of the bed deformation increasing and the damping decrease for decreasing $f(\theta_0)$.

In figure 12 results of computations with p=0 and p=1, but the same value of $f(\theta_0)$ are depicted. On first sight the difference between the two curves is not in accordance with equation (45). This is because the depths in the axis of the two computations are not equal and furthermore upstream effects which is not included in equation (45) also play an important role in the present case where $v \neq 0$ and $\tan\psi \neq 0$. The remaining models for the influence of the bed slope on the sediment transport direction would yield results in between the two curves in figure 12. The figure illustrates that even in the present case of a sharply curved bend the influence of the spatial variation of $f(\theta)$ is relative small. However, the averaged value of this term has a very large influence on both the fully developed bed topography, i.e. zero-order solution, and on the developing bed topography (first order solution, cf. figure 2). Only few experiments from which the value of $f(\theta_0)$ can be obtained directly have been carried out. In most experiments the quantity $a/f(\theta_0)$ has been measured and, regarding the reliability of a (i.e. the magnitude of the secondary flow), the value of $f(\theta_0)$ is poorly determined. This makes $f(\theta_0)$ an obvious tool for calibration of the model.

Also the angular difference between the velocity vector near the surface and near the bed was measured. Based on a logarithmic distribution of the longitudinal flow velocity and a parabolic distribution of the eddy viscosity de Vriend (1976) obtained an expression for the vertical

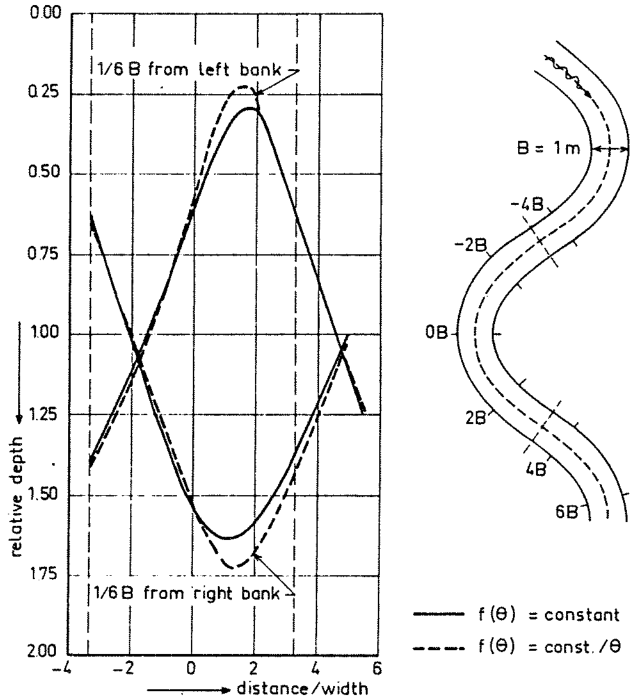

Figure 12. Influence of the model for the gravitational effect.

distribution of the secondary flow. According to de Vriend (1976) the direction of the flow near the bottom is given by eq.(9) and the direction of the surface flow by

$$\tan \delta_{surf} = \frac{1}{\kappa^2} \frac{1.2899 - 2.404 \frac{\sqrt{g}}{\kappa C} + 2 \frac{g}{\kappa C^2}}{1 + \frac{\sqrt{g}}{\kappa C}} \frac{h}{R_s} \qquad (46)$$

The maximum measured angle was in between 30° and 35°, measured at a location in the flume where the depth was about 0.16 m. The radius of curvature of the streamlines at this specific location have been estimated from a numerical computation to about 2 m . Inserting these values for h and $1/R_s$ in the theoretical expressions for the flow direction yield $\tan(\delta+\delta_{surf})=1.3$; whereas the measurements suggest $\tan(\delta+\delta_{surf})=0.65$. Consequently, the theoretical model seems to overestimate the magnitude of the secondary flow with a factor two.

Hence, in the numerical computations for the experiment a=4.3 (i.e. $\tan\delta=4.3h/R$) will be applied.

Actually, it is quite surprising that the theoretical model overestimates the magnitude of the secondary flow as recent measurements of the secondary flow in flumes with hydraulic smooth bed indicates that the theoretic model underestimates the secondary flow (cf de Vriend, 1981). This discrepancy may be attributed to difference in vertical distribution of the longitudinal flow velocity and of the eddy viscosity in case of hydraulic smooth and alluvial (rough) bed.

In figure 13 a computation, with the measured magnitude of the secondary flow (a=4.3) and the value of $f(\theta_0)$ (1.35) which gives the best agreement with the measured data, is depicted. A larger value of $f(\theta_0)$than 1.35 will cause a slight upstream shift of the point bar and pool, i.e. an improved phase, but at the same time the transverse slope will decrease resulting in an inferior over-all agreement. For a value smaller than 1.35 there is no solution of the mathematical model, because, in the flow model above the point bar the energy-line descends below the water surface. Physically, it probably means that the point bar will emerge through the water surface, i.e. the width will locally decrease.

The agreement between the measured and (the best) calculated bed topography in figure 13 could be better. Comparison of the measured and computed sediment transport distribution shows that the theoretical model underestimates the transverse gradient of the longitudinal sediment transport rate and that the location where the sediment transport maximum crosses from the convex to the concave banks of the flume is situated too far downstream (measured 1/4B downstream of the apex, computed 1 1/2B). This, of course, results in large differences in distribution of transverse sediment transport, which is so essential for the bed topography (cf. Struiksma et al, 1985).

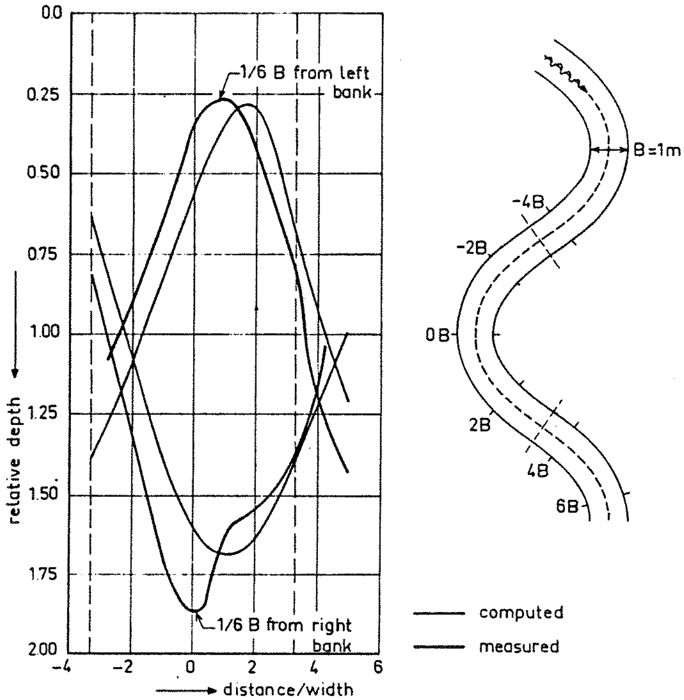

Figure 13. Comparison of computated and measured bed level.

The cause of the inferior sediment transport distribution may partially be attributed to a bad sediment transport model; but, in view of the bad prediction of the position of the sediment transport crossing, it is likely to assume that also the flow velocity distribution is incorrectly predicted. A flow model, that includes the effect of secondary flow convection, would lead to a larger flow velocity near the concave bank; so, the velocity maximum would shift from the convex to the concave bank further upstream and in most cross-sections the transverse gradient of the longitudinal flow velocity would increase. Both effects would lead to an improved sediment transport distribution and therefore probably also a better bed topography prediction.

The effect of secondary flow convection can be simulated in a rough way by manipulations with the alluvial roughness coefficient. However, as the flow velocity distribution was not measured in the experiment, such excercises have not been carried out in this case.

The main features of the bed topography, viz. the position of the point bar downstream of the apex of the flume is qualitativly correctly reproduced by the computational model, but the distance lag is overestimated. For the present case of a sharply curved bend the flow model seems to be insufficiently refined, namely the influence of the spiral (secondary) flow on the main flow distribution is not incorporated.

4.2. Experiment in the DHL curved flume

The experiment is carried out at the Delft Hydraulics Laboratory in a 1.5 m wide flume consisting of a 7 m long straight inflow section preceeded by a 140^{o} bend with a centerline radius of curvature of 12 m and an 11 m long straight outflow section. The bed level data are based on the mean value of 25 soundings carried out during the equilibrium state, that was obtained after flowing two weeks, so the measured bed topography can be considered unconditional stationary. During the equilibrium state also the flow velocity was measured in some selected cross-sections. These measurements were carried out with current meters of the micro-propeller type. The monitoring period was 1000 s and each measurement was carried out four times in order to improve the accuracy. Still, it is not certain that the mean value of the measurements actually represent the mean flow velocity, because of the "noise" of the slowly propagating bed forms.

A rather uniform sediment with a geometrical mean value of 0.45 mm was used in the experiment. Sediment transport measurements in this experiment and in a few others in which the same sediment was used exhibit a good agreement with the Engelund-Hansen (1967) sediment

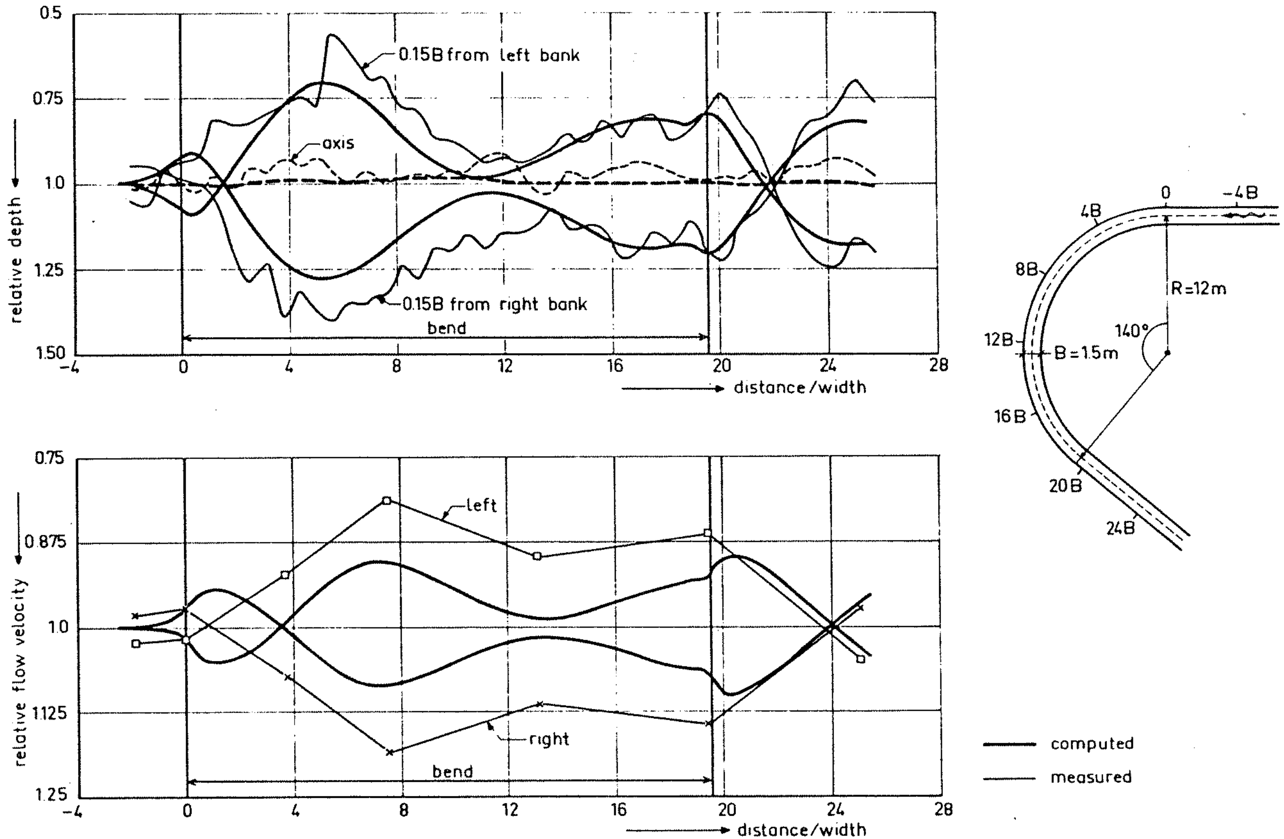

Figure 14. Computed and measured bed level and flow field in the DHL curved flume.

transport formula (i.e. b=5). An impression of the bed form height can be obtained from the standard deviation of the bed soundings. It appears that the bed form height - water depth ratio is approximately constant implying that the bed roughness is constant (i.e. no spatial variation).

For a detailed outline of the model features, measuring procedures and results see Struiksma (1983 b). The relevant hydraulic and geometric data for the experiment are summarized in table 1. In figure 14 the measured bed topography and, due to the scatter in the flow velocity measurements, the mean value of the depth averaged flow velocity left and right of the flume axis are depicted.

4.2.1. Calibration of the model

The relative large wave length of the measured bed deformations (cf. figure 14) indicates that computational results will be insensitive to the numerical value of the slope coefficient in the model for the longitudinal sediment transport rate and insensitive to the magnitude of the adaption length of the secondary flow. This can be verified by the linear analysis and it has also been verified with some preliminary computations (not depicted). Therefore, in order to enable a large time step in the computations, a relative large longitudinal slope coefficient and adaption length of the secondary flow has been applied (cf. appendix B).

Struiksma et al (1985) show that it is necessary to apply $\lambda_w/\lambda_a\pi^2 = 0.68$ in order to obtain a realistic wave length of the bed deformations. This value is obtained with $f(\theta_0)=1.25$. By estimating the axial symmetric bed slope from the measured data the quantity $a/f(\theta_0)$ can be obtained from equation (45). In figure 14 results of a computation with $a/f(\theta_0)=2.7$, i.e. a=3.4 which is only about 40 % of the theoretical value, is depicted. The transverse bed slope in the first say 2/3 of the bend is underestimated whereas the transverse slope in the last part of the bend

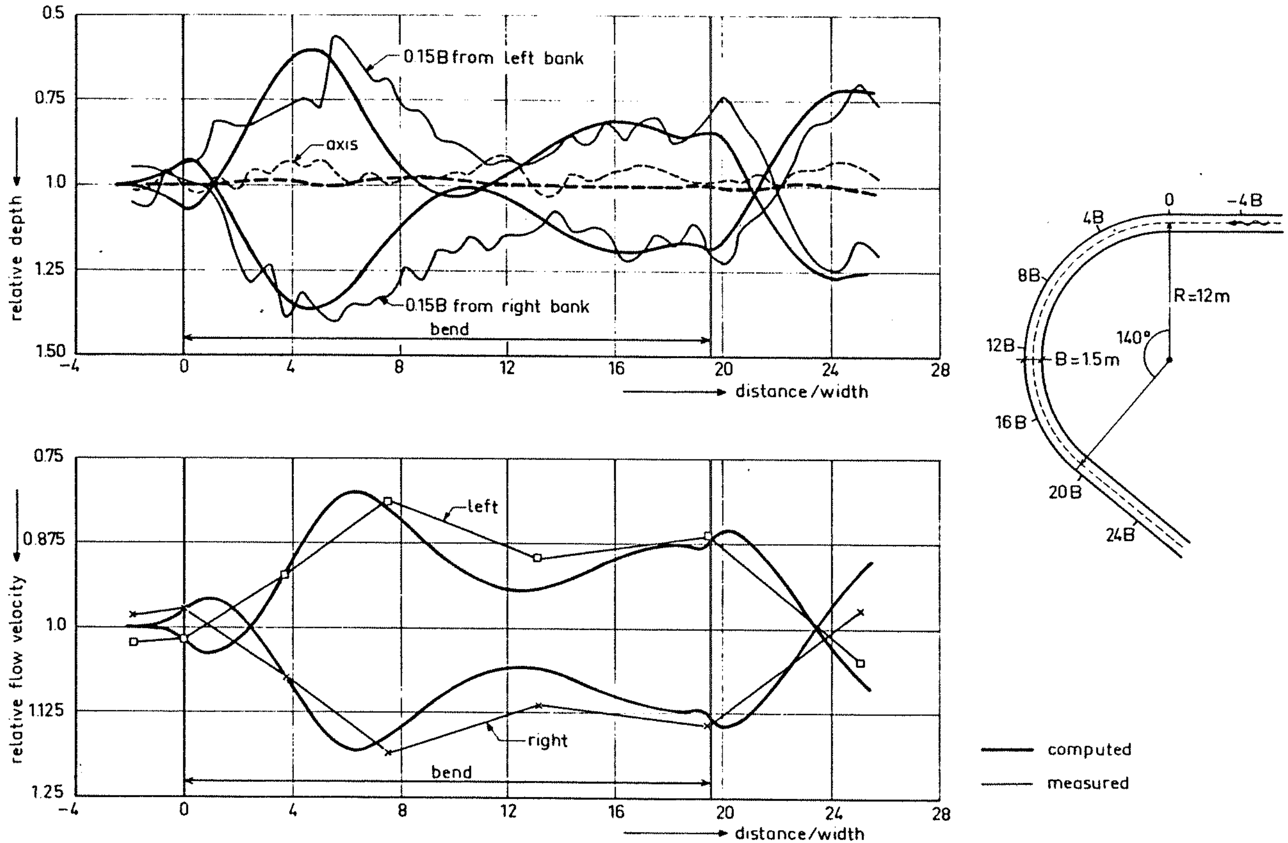

Figure 15. Computed and measured bed level and flow field in the DHL curved flume. Improved flow field.

is very well predicted. The transverse gradient of the flow velocity is systematically underestimated, probably due to the omisson of secondary flow convection in the flow model. The distance lag between the flow and bed deformation seems reasonably well predicted.

According to Kalkwijk & de Vriend (1980) and de Vriend & Struiksma (1983) the influence of secondary flow convection depends on two different length scales, viz. on $C^2/2g$ h and on BR/h . The first length scale equals λ_w i.e. the length scale from the main flow model, so this effect can adequately be accounted for by introducing a transverse variation of the bed roughness coefficient. The second length scale is very large, in the present case about 180 m., so this effect can be neglected.

It is assumed that the transverse variation of the roughness coefficient is linear and proportional with h/R in the channel axis. The aim of the tuning is to obtain the correct order of magnitude of the transverse gradient of the longitudinal main flow velocity, and for this purpose this approach is assumed sufficient refined. The order of magnitude of the variation of the rougness coefficient is obtained from Chezy's law using the measured flow velocity and bed topography data. In figure 15 the result of a computation with the calibrated coefficient and the tuned flow model is depicted. Compared with figure 15 it is seen that the prediction of the point bar height and pool depth are improved. Also the flow field is in better agreement with the measured data. However, the wave length is shorter, the point bar/pool is shifted upstream and there is a significant lag between the predicted and calculated point bar/pool. Furthermore, the damping of the oscillating bed deformation is far too small.

According to the linear analysis an improved prediction of the wave length of the bed deformation requires a reduction of $f(\theta_0)$, but this will inevitably cause less damping of the bed deformation resulting in a greater disagreement with the measured data around s=13 B. The only way to obtain significant further decay of the bed deformation is to reduce

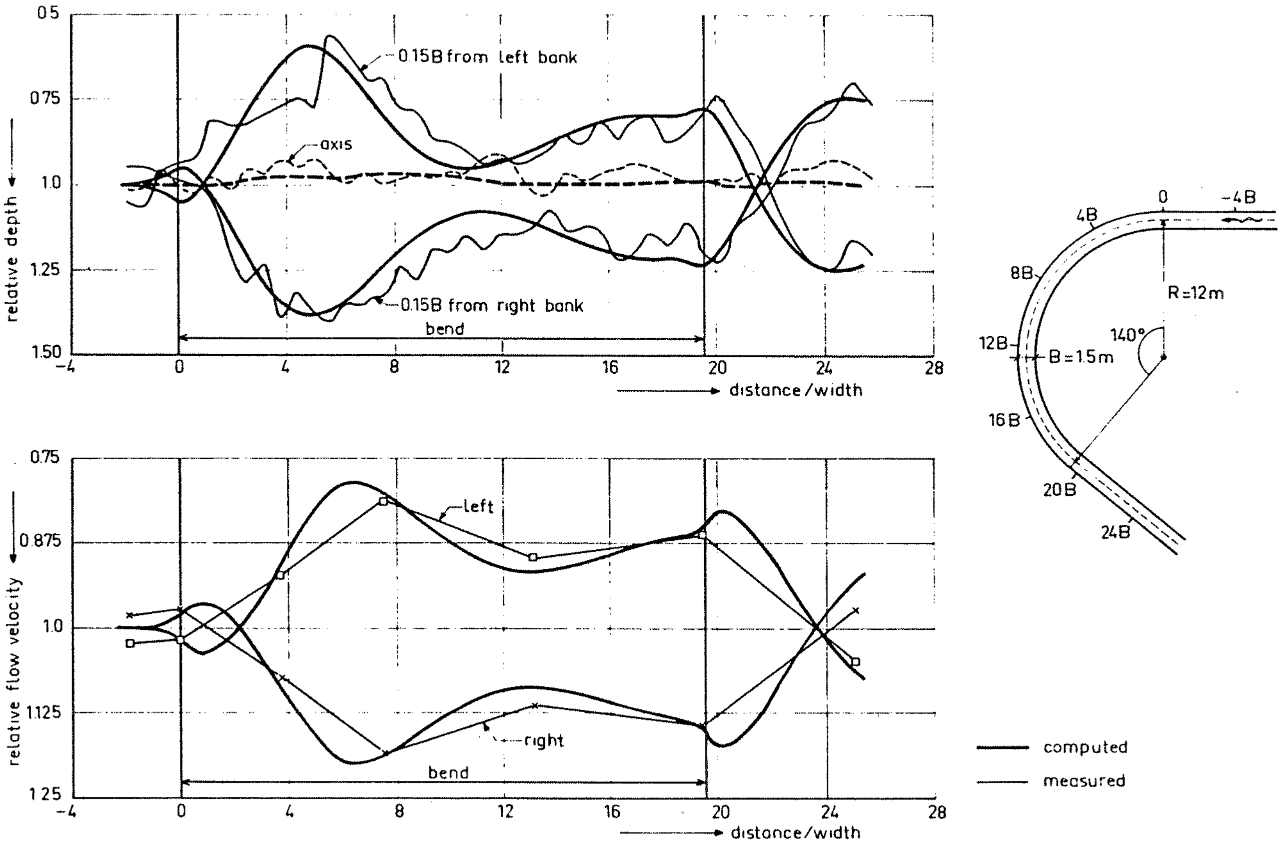

Figure 16. Computed and measured bed level and flow field in the DHL curved flume. Improved flow field and calibrated sediment transport model.

the power, b, in the sediment transport formula. In figure 16 results of a computation with a=4, b=4, $f(\theta_0)=1$ and the tuned flow model is depicted. The result now agrees much better with the measured data. However, in view of the sediment transport measurements in the present experiments and in other experiments with the same sand (all indicating that - on the average - b=5), it does not seem likely to assume that b=4. On the other hand, the variation of the sediment transport rate in trnsverse direction is very large (larger than the range of sediment transport rate in the above mentioned experiments), so b may not be constant over the width. The influnce of such a spatial variation of b on the bed topography is not clear yet.

Due to the many (physical plausible) calibration possibilities, it will almost always be possible to obtain a reasonable agreement with the measured data. Even without a reasonable flow field prediction a good agreement with the measured bed topography can be obtained by manipulation with the model parameters a, b and $f(\theta_0)$. Consequently, for an integral verification of the mathematical model a rather extensive measuring programme has to be carried out. Besides bed topography, roughness, discharge and sediment transport measurements, a flume experiment well suited for calibration of the model, should involve flow measurements. Furthermore, it is also very attractive to have a good estimate of at least one of the three model parameters: a, b or $f(\theta_0)$. Even in case of straight uniform flow it is difficult to obtain an unambiguous functional relationship between the flow and sediment properties (i.e. b; cf. the large number of existing sediment transport formulas) and the direction of the bed shear stress in a curved flow with moveable bed is hardly feasible to measure accurately so experimental verification of $f(\theta_0)$ is probably the option which often the best prospects. Ikeda (1981), Fredsoe (1976) and Zhaohui (1976) have attempted to measure $f(\theta_0)$ in a straight flow, i.e. they did not have to assume a model for the direction of the bed shear stress. In the experiment they began with a transverse slope in a long straight flume. In this case all derivatives in longitudinal direction and the transverse velocity can be assumed to vanish so the mathematical model transforms into Chezy's law and

$$\frac{\partial h}{\partial t} = \frac{\partial}{\partial n} (S_x \; f(\theta) \; \frac{\partial h}{\partial n}) \tag{47}$$

By measuring the sediment transport rate and the transverse slope as a function of time $f(\theta_0)$ can be obtained. So far this method probably offers the best prospects, but a large number of experiments still have to be carried out before an unambiguous relation can be determined.

4.3. The river Dommel

The last test case concerns the small Dutch-Belgium river Dommel, a contributor to the Meuse. Bed geometry and flow velocity measurements were carried out in May 1980 in a 285 m long section of the river. All relevant data concerning bed topography, main flow velocity and water surface level have been reported by de Vriend & Geldof (1983). Data concerning sècondary flow and sediment properties have been reported by van Alphen, Bloks and Hoekstra (1985).

The geometry of the river bed was surveyed twice, in the periods 1-5 May and 27-28 May 1980, by levelling along 52 traverses. Only small differences were found between the two levellings. In the present investigation the first series of measurements is used. The influence of bed forms (mostly ripples, locally dunes), with a maximum height estimated to about 0.1 m., were not eliminated by averaging a large number of levellings at each point.

Extensive flow measurements were performed. The main flow velocity was measured with a propeller type current meter in 14 to 25 points in 23 cross-sections. The secondary flow was measured in some selected cross-sections by simultaneous measuring two horizontal velocity components in a vertical with an electro-magnetic current meter.

The water level was measured twice a day at four point gauge stations along the considered area. Furthermore, 150 m upstream of the considered area a Rijkswaterstaat float gauge station is situated which registrates the waterlevel each quarter of an hour.

In addition, extensive measurements of the sediment properties were carried out.

4.3.1. River schematization

Several problems arise when the numerical model is applied to a natural river such as the Dommel, viz.

- The abcense of well defined steady flow conditions requires a choice of a dominant discharge and water surface level. Especially, it is important to choose a representative water surface level as the depth width ratio has a large influence on the predicted bed topography. The discharge, or rather, the overall mean flow velocity has only influence on the equilibrium bed topography through the terms $f(\theta_0)$ (cf. equations (12) through (18)), which anyway is used as a calibration quantity. Furthermore, the flow velocity (through the sediment transport model) has a large influence on the time scale on which the bed level changes take place (cf. equation 5).

- The planform of the river is difficult to schematize. The width varies along the river and with the water surface level, e.g. in case of low flow, the situation in which the survey took place, the point bars will not be submerged. This implies that the position of the river axis is poorly defined and therefore also the curvature of the river. Furthermore, the river does not have vertical banks.

- Vegetation at the banks and in the river bed and other non-alluvial roughness elements influence the flow distribution and hence the sedimentation stuctures.

- The river has rather graded sediment.

Pilot computation with the model indicated that the time needed for establishment of equilibrium starting from horizontal bed is of the order of magnitude 20 m^2/S_o. The sediment transport rate in the river was measured by means of dune tracking about a year after the data used

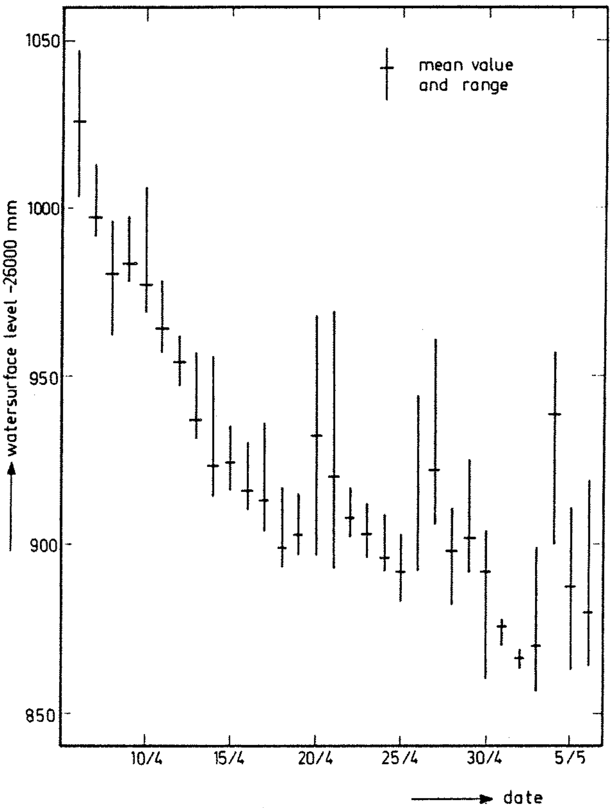

Figure 17. Variation of the water surface level.

in this report were sampled. During the sediment transport measurements the flow situation was quite similar to the one used here. The result of the measurements indicates a transport rate of about 0.5 m^2/day which corresponds to a real time to obtain equilibrium of about 40 days. In figure 17 the variation of the water surface level at the Rijkswaterstaat float gauge station prior and during the survey period has been depicted. The representative (dominant) water surface is probably larger than the averaged water level as large flow velocities and hence sediment transport rates occur during high stages. On the other hand the water level in the period short before and during the survey period has larger influence on the observed bed topography so these data should be attached more weight. Based on these considerations a water surface level of 26950 mm is (somehow arbitrary) chosen. This water surface level corresponds to a mean depth of about 0.6 m and a mean flow velocity of about 0.55 m/s.

The local width of the river and the coordinates of the river axis were determined by means of the bed profile diagrammes depicted in de Vriend & Geldof (1983). For each of the bed profiles the part of the river bed which does not seem influenced by the banks were estimated. The width of the river, estimated in this way, varied from 4.1 m. until 6.1 m. with a mean value of about 5 m which will be used in the computations. The deviation from the mean width is not unsystematical; there was a significant trend that the width is inreasing in the flow direction. It is not quite clear whether the applied procedure yields the optimal width of the river for the computations.

The centerline curvature of the river was obtained from the river axis by constructing circles through the axis of three successive cross-sections. The curvature obtained in this way exhibited a relative large scatter and was not equaly spaced, so the data were interpolated into a regular grid and smoothed by applying a moving average. In figure 18 the centerline curvature before and after the smoothing and spacing are depicted.

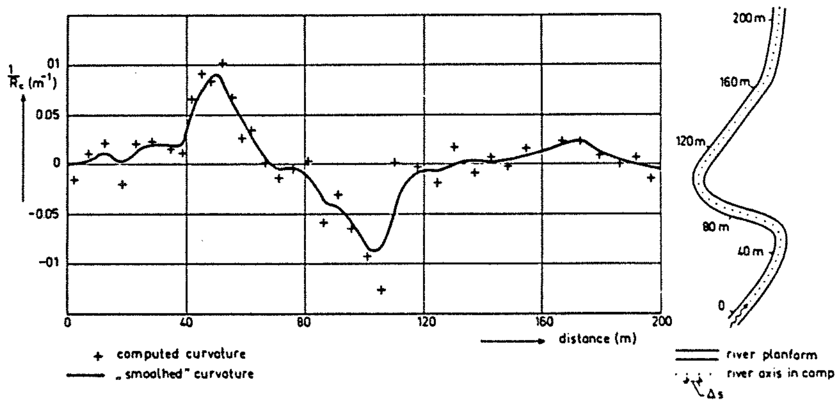

Figure 18. Schematized center line curvature of the river.

Longitudinal bed profiles at 1/4 B from the banks were estimated from the bed diagramms in de Vriend & Geldof (1983) and are depicted in figure 19. Longitudinal profiles closer to the banks would exhibit an even larger scatter than the profile depicted in figure 19 due to for instance banks vegetation and local bank failure. At s=20 B vegetation was found in the bed which locally, but also downstream of the pool/point bar influences the bed considerably.

The bed material is quite graded. In the straight reaches the mean diameter varies from 0.37 mm to 0.51 mm. In the bends the mean diameter varies from about 0.2 mm close to the inner (convex) banks to 1.4 mm close to the concave banks. The overall mean value is about 0.47 mm. The rather pronounced spatial variation of the mean grain size has a large influence on the sediment transport rate, so significant influence on the bed topography can be expected.

4.3.2. Calibration of the model

The flow field in a river as the present one is to a large extent controled by the bed friction. Consequently, the flow field is stage dependent which makes the profound flow measurements carried out in the Dommel at a lower stage less suitable for direct calibration of the flow model in the present case. de Vriend & Geldof (1983) find, using in principle the same flow model as the one used here, that secondary flow convection only has influence on the flow field near the exit of the relative short bends in the Dommel. This is supposed to apply in the present case as well.

The secondary flow measurements can be used to check the theoretical model for the magnitude of the secondary flow. The measurements indicate a maximum angular difference of 30° ($\tan 30^{\circ}=0.58$) between the flow vector at the surface and the bed whereas the theoretical model, i.e. equations (9) and (46), suggest an angle of about 50° ($\tan 50^{\circ}=1.2$). So, also in this case the theoretical model for the secondary flow seems to overestimate the actual value with a factor of about two. In view of this a=4.6 is applied in the computations.

No analysis of the sediment transport rate data has been carried out in order to facilitate the choice of a sediment transport formula. It is simply assumed that the Engelund-Hansen transport formula applies in the Dommel. Several computations with different $f(\theta_0)$ have been carried out. It appeared that computations with $f(\theta_0)<1.3$ failed because the water depth above the point bars in the bends tends towards zero, i.e. the point bars emerge through the water surface. This implies that the width locally decreases; a trend, which, - especially in the first bend - can be detected in the measured data as well.

In figure 19 the measured data and results of a computation with $f(\theta_0)=1.3$ are depicted. The agreement is not very good. The point bar height/pool depth in the first bend is underestimated whereas it is overestimated in the second bend. Actually it is not possible to choose a parameter combination resulting in a larger transverse bed gradient in the first bend than in the second bend. This discrepancy with the measured data may be attributed to variation of the width and on the bed vegetation in the second bend. The width, estimated by means of the bed

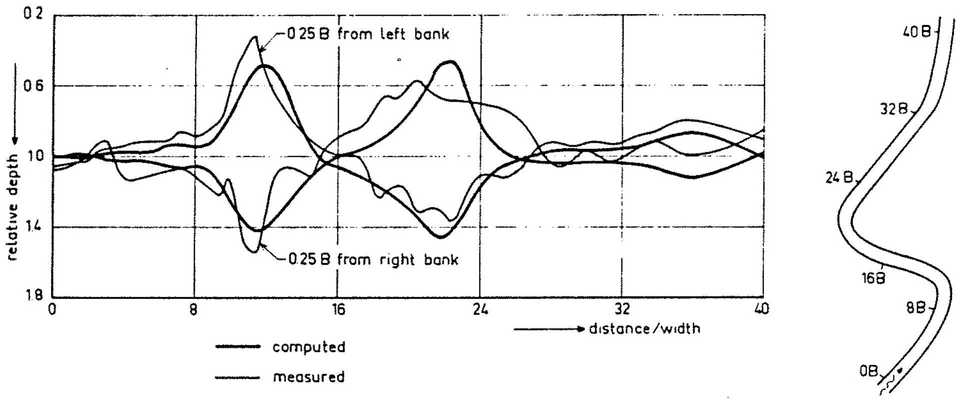

Figure 19. Computed and measured water depth.

profile diagramme in de Vriend & Geldof (1983), is smaller around the point bar in the first bend than in the second bend which may be the reason for the larger transverse bed gradient in the first bend. The vegetation in the bed forms an additional roughness element and in this way it influences the flow distribution. This will have considerable influence on the sediment movement and therefore also on the bed topography. In the last part of the reach, say s>28 B, the measured depth is systematically larger than the computated. This is caused by a larger width (smaller mean depth) in that reach of the river. Consequently, a model with variable width is necessary in order to improve the computation results at that point.

The position of the crossings are rather well predicted by the model. Furthermore, as the measured longitudinal bed profiles are based on only one sounding, the deviation between the measured and computated bed topography may to some extend be attributed to the bed form (i.e. random scatter).

So far most attemps to compute the bed topography in river bends have been based on the assumption that the sediment transport is parallel to the river axis.This is more or less tantamount to the present model with b=0, i.e. the sediment transport is constant. According to the linear

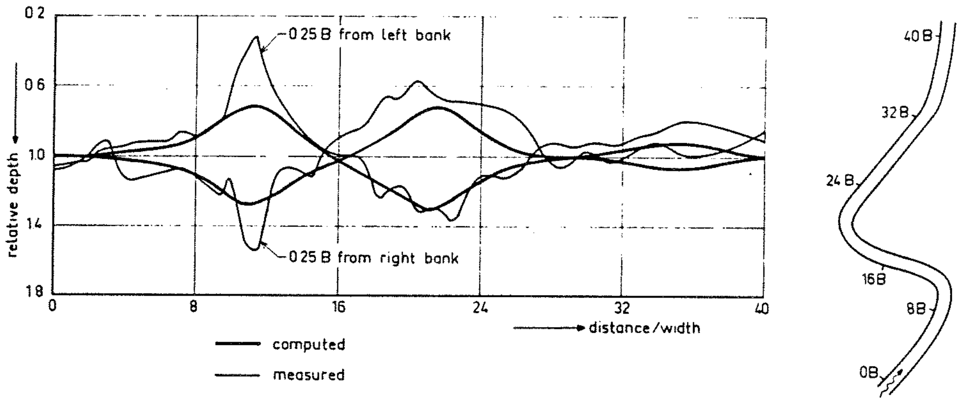

Figure 20. Computed and measured water depth. Influence of redistribution of the sediment transport (b=0).

analysis (equation 28) this is mostly a very bad approximation, except maybe in a strongly damped system, i.e. rivers with a small width-depth ratio. In the Dommel this ratio is relative small. In order to investigate whether bed level prediction with the simplified model (sediment transport parallel to the river axis) yields a realistic result a computation with constant longitudinal sediment transport was carried out. The remaining variables were as in the computation depicted in figure 19. In figure 20 the result of this computation is depicted. The difference with figure 19 is very significant. Consequently, even in case of a very small width-depth ratio, the spatial variation of the sediment transport cannot be neglected.

5. Discussion and conclusions.

The equilibrium bed topography in an alluvial river bend is,in the mathematical model,governed by mutual interaction between the bed shear stress distribution and the sediment transport distribution. In view of the relatively good agreement between measured and computed bed topography in the cases discussed, it can be concluded that the mathematical model includes the fundamental aspects of the system of flowing water and moving sediment, and also that the interaction between the components are adequately desribed. However, the necessary calibration of the model illustrates that the model contains some shortcomings.

Two aspects are of particular importance for a good bed shear stress description, viz. an adequate flow model and a good description of the roughness distribution. The theoretical model for the bed shear stress direction in a curved flow, which is based on the assumption of a parabolic eddy viscosity distribution and uniform flow, seems to overestimate the direction of the bed shear stress vector in the three cases considered. It appears that in large natural rivers the model works well (Struiksma, personal communication). Generally, a characteristic difference between an experimental flume and a large natural river is the water depth dune height ratio, which is much smaller in the flume. It is likely that the assumption of a parabolic eddy viscosity distribution becomes less valid when the relative bed form height becomes larger. Furthermore, the flow will become less uniform. Consequently, it is not surprising that the theoretical model is less reliable in a shallow flume. Further research on the secondary flow over an alluvial bed is necessary; possibly experimental by measuring the shear stress distribution in the flow around a bed form. Another possibility to improve the bed shear stress direction model is to make a numerical investigation using a 2-dimensional (vertical) model, or perhaps a fully 3-dimensional model, with a more sophisticated eddy viscosity model than the parabolic one.

The flow model applied in the mathematical model neglects the influence of secondary flow convection, which at least in some cases, has significant influence on the main flow distribution. It appears that the effect of secondary flow convection can be approximated in the computational model by introducing a lateral varying roughness coefficient, but the degree of variation is still a matter of calibration.

Even if the bed shear stress distribution is well known, the sediment transport magnitude and distribution are difficult to determine. The computation with different sediment transport predictors (different "b", see figures 15 and 16) underlines the importance of reliable sediment transport formulas. In the past few decades much effort has been put in the investigation of the sediment transport mechanisms, without any spectacular improvement of the reliability of the sediment transport predictors. So it is inevitable that the choice of a sediment transport formula for the mathematical model will remain a matter of calibration.

The model describing the influence of (transverse) bed slope on the sediment transport direction is very important. In combination with the model for the bed shear stress direction it determines the axial-symmetric (average) bed slope in a bend and it has a large influence on the "overshoot" phenomena in areas of transient curvature, i.e. the model determines the response of the equilibrium bed to angular differences between the sediment transport and the bed shear stress. The above mentioned comments on the sediment transport rate predictors also apply to the model for the slope dependence of the sediment transport direction. In view of the dominant influence of this model on the bed topography in rivers it is essential to attempt to obtain more knowledge about it. As mentioned in Chapter 3 independent (not in corporation with a model for the transverse bed shear stress in acurved flow) determination of this term can (so far) only be done using unsteady experiments. In spite of the experimental difficulties involved much more experiments of this kind should be carried out in order to improve the reliability of the prediction of the sediment transport direction.

Summarizing, it can be concluded that the mathematical model contains the essential components for a proper description of the bed topography in rivers. However, the insufficient reliability of the models for -(1) the bed shear stress direction in a curved flow, -(2) secondary flow convection in channels with vertical banks, -(3) the sediment transport rate and -(4) the sediment transport direction on a sloping bed make calibration of the model necessary.

REFERENCES

ALPHEN J.L.S.J.VAN, BLOKS P.M. & HOEKSTRA P. (1985) "Flow and grainsize pattern in a sharply curved river bend", Earth surface processes and landforms", Vol. 9, p. 5/3.

BENDEGOM L.VAN (1947) "Some considerations on river morphology and river improvement", De Ingenieur, Vol. 59, No. 4, (in dutch; english transl.: Nat. Res. Counc. Canada, Tech. Transl. 1054, 1963).

BOOIJ R. & KALKWIJK J.P.TH. (1982) "Secondary flow in estuaries due to the curvature of the main flow and to the rotation of the earth", Report 9-82, Lab. Fluid Mech., Dept. Civil Engng., Delft Univ. Techn., Delft, the Netherlands.

ENGELUND F. (1974) " Flow and bed topography in channel bends", J. Hyd. Div., ASCE, Vol. 100, No. HY11, p. 1631.

ENGELUND F. (1981) "The motion of sediment particles on an inclined bed", Prog. Rep. 53, Inst. Hydrodyn. and Hydraulic Engng., Tech. Univ. Denmark, April 1981, p. 15.

ENGELUND F. & HANSEN E. (1967) "A monograph on sediment transport in alluvial streams", Copenhagen, Danish Technical Press.

FREDSOE J. (1976) "Levelling of side slopes in river navigation channels", Prog. Rep. 38, Inst. Hydrodyn. and Hydraulic Engng., Tech. Univ. Denmark, April 1976, p. 9.

HOOKE R.L. (1975) "Distribution of sediment transport and shear stress in a meander bend", J. Geology, Vol. 83, No. 5, p. 543.

IKEDA S. (1981) "Lateral bed load transport on side slope", Rep. of Dept. Fundation Engng. and Dept. Constr. Engng., Saitama Univ., Japan, August 1981.

JANSEN P.PH. (1979) "Principles of river engineering", Pitman Publ., London.

KALKWIJK J.P.TH. & VRIEND H.J.DE (1980) "Computation of the flow in shallow river bends", J. Hydr. Research, Vol. 18, No. 4, p. 327.

KIKKAWA H., IKEDA J. & KITAGAWA A. (1976) "Flow and bed topography in curved open channels", J. Hyd. Div.,ASCE, Vol. 102, No. HY9, p. 1327.

ODGAARD A.J. (1981) "Transverse bed slope in alluvial channel bends", J. Hyd. Div., ASCE, Vol. 107, No. HY12, p. 1677.

OLESEN K.W. (1982 a) "Influence of secondary flow on meandering of rivers", Delft Univ. Tech., Dept. Civil engng., Lab. Fluid Mech., Report No. 1-82.

OLESEN K.W. (1982 b) "Introduction of streamline curvature into flow computation for shallow river bends", Delft Univ. Tech., Dept. Civil Engng., Lab. Fluid Mech., Report No. 5-82.

OLESEN K.W. (1983) "Alternate bars in and meandering of alluvial rivers", Presented on a speciality conference on river meandering, RIVERS '83, ASCE, New Orleans. Also as Communications on Hydraulics 83-1, Delft Univ. Tech., Dept. Civil Engng.

ROZOWSKII I.L. (1957) "Flow of water in bends of open channels", Israel Progr. for Scientific Transl., Jerusalem 1961.

STRUIKSMA N. (1983 a) "Point bar initiation in bends of alluvial rivers with dominant bed load transport", TOW, Report R657 - XVII/W308 - PART III, Delft Hydraulics Lab., the Netherlands.

STRUIKSMA N. (1983 b) "Results of movable bed experiments in the DHL curved flume", Report on Experimental Investigation, TOW, Report R657 - XVIII/M1771, Delft Hydraulics Lab., the Netherlands.

STRUIKSMA N., OLESEN K.W., FLOKSTRA C. & VRIEND H.J.DE (1985) "Bed deformation in alluvial channel bends", J. Hyd. Research, Vol. 23 , No. 1, p.57.

VRIEND H.J. DE (1976) "A mathematical model of steady flow in curved shallow channels", Delft Univ. Tech., Dept. Civil Engng., Communications on Hydraulics 76-1.

VRIEND H.J.DE (1978) "Developing laminar flow in curved rectangular channels", Delft univ. Tech., Dept. Civil Engng., Lab. Fluid Mech., Internal Report 6-78.

VRIEND H.J.DE (1981) "Steady flow in shallow channel bends", Delft Univ. Tech., Dept. Civil Engng., Communications on Hydraulics 81-3, (also as doctoral thesis of Delft Univ. Tech., 1981).

VRIEND H.J.DE & GELDOF H.J. (1983) "Main flow velocity in short and sharply curved river bends", Delft Univ. Tech., Dept. Civil Engng., Communications on Hydraulics 83-6.

VRIEND H.J.DE & STRUIKSMA N. (1983) "Flow and bed deformation in river bends", Presented on a speciality conference on river meandering, RIVERS ´83, ASCE, New Orleans.

ZHAOHUI W. (1981) "The deformation of a sand bed with a transverse slope", Prog. Rep. 55, Inst. Hydrodyn. and Hydraulic Engng., Tech. Univ. Denmark, April 1981, p. 9.

Appendix A. Discretization of the bed level model

In the numerical integration procedure for the bed level model central space differences are applied (except at the boundaries) and the time derivative is approximated with an explicit first order difference.

The finite difference approximation of the equation of continuity can be obtained by formal integration over a box around the point (m,j) in the computational grid. The result is

$$\left(\frac{\partial h}{\partial t}\,\Delta s\right)[m,j]\,\Delta n = \left(S_s[m+\tfrac{1}{2},j] - S_s[m-\tfrac{1}{2},j]\right)\Delta n + (S_n\Delta s)[m,j+\tfrac{1}{2}] - (S_n\Delta s)[m,j-\tfrac{1}{2}] \qquad \text{(A1)}$$

At the boundaries this scheme does not apply. Therefore, at the inflow section the depth is kept constant and at the inner wall the following non-central difference approximation is applied

$$\left(\frac{\partial h}{\partial t}\,\Delta s\right)[m,1] = \left(S_s[m+\tfrac{1}{2},1] - S_s[m-\tfrac{1}{2},1]\right)\Delta n - 2\,S_n[m,\tfrac{3}{2}] \qquad \text{(A2)}$$

recalling $S_n[m,1] = 0$. At the outer wall a similar scheme is used. At the outflow boundary the following finite difference approximation is applied

$$\left(\frac{\partial h}{\partial t}\,\Delta s\right)[M,j]\,\Delta n = 2\left(S_s[M,j] - S_s[M-\tfrac{1}{2},j]\right)\Delta n + (S_n\,\Delta s)[M,j+\tfrac{1}{2}] - S_n\Delta s[M,j-\tfrac{1}{2}] \qquad \text{(A3)}$$

The longitudinal transport rate has to be calculated in the staggered grid, viz.

$$S_s[m+\tfrac{1}{2},j] = \{(u[m+1,j] + u[m,j])/2\}^b \{1+\alpha(h[m+1,j]-h[m,j])/\Delta s[m+\tfrac{1}{2},j]\} \qquad \text{(A4)}$$

The direction of the sediment transport is obtained from

$$\tan\psi[m, j+\tfrac{1}{2}] = \{(v[m+\tfrac{1}{2}, j] + v[m-\tfrac{1}{2}, j])/u[m, j]$$

$$+(v[m+\tfrac{1}{2}, j+1] + v[m-\tfrac{1}{2}, j+1])/u[m, j+1]$$

$$+ \tan\delta^*[m+\tfrac{1}{2}, j] + \tan\delta^*[m-\tfrac{1}{2}, j] + \tan\delta^*[m+\tfrac{1}{2}, j+1] + \tan\delta^*[m-\tfrac{1}{2}, j+1]\}/4$$

$$+ f(\theta[m, j+\tfrac{1}{2}])(h[m, j+1] - h[m, j])/\Delta n \qquad \text{(A5)}$$

in which the direction of the bed shear stress in a curved flow, $\tan\delta^*$, is obtained from

$$\tan\delta^*[m+\tfrac{1}{2}, j]\{(\lambda_{sf}/\Delta s)[m, j] + \tfrac{1}{2}\} = \tan\delta^*[m-\tfrac{1}{2}, j]\{(\lambda_{sf}/\Delta s)[m, j] - \tfrac{1}{2}\}$$

$$- a\frac{h}{R_s}[m, j] \qquad \text{(A6)}$$

Last, the transverse sediment transport rate is approximated by

$$S_n[m, j+\tfrac{1}{2}] = \tan\psi[m, j+\tfrac{1}{2}](S_s[m+\tfrac{1}{2}, j+1] + S_s[m+\tfrac{1}{2}, j]$$

$$+ S_s[m-\tfrac{1}{2}, j+1] + S_s[m-\tfrac{1}{2}, j])/4 \qquad \text{(A7)}$$

The various finite difference approximations are depicted in the computational grid in Figure 4.

	Hooke				DHI. curved flume			Dommel	
Figure	10	11	12	13	14	15	16	19	20
$\Delta x/B$	0.55	0.55	0.55	0.55	0.63	0.63	0.63	0.83	0.83
$\Delta y/B$	0.17	0.17	0.17	0.17	0.25	0.25	0.25	0.25	0.25
$\Delta t h_*^2/S_*$	0.22	0.22	0.22	0.22	0.47	0.47	0.47	0.14	0.14
β^+	0.6	0.6	0.6	0.6	0.9	0.9	0.9	0.6	0.6
α	5	5	5	5	8	8	8	5	5
a	7.0	7.0	5.8	4.3	3.4	3.4	3.4	4.6	4.6
$f(\theta)$	1.96	1.96	1.66;0.7/θ	$0.87/\sqrt{\theta}$	$0.64/\sqrt{\theta}$	$0.64/\sqrt{\theta}$	$0.64/\sqrt{\theta}$	$0.86/\sqrt{\theta}$	$0.86/\sqrt{\theta}$
b	4	4	4	4	5	5	4	5	0

+) $\lambda_{sf}=\beta C/\sqrt{g}\,h$

Appendix B - Computational "details"